Chapter 1
Bioinspired Nanoscale Water Channel and its Potential Applications

Haiping Fang, Chunlei Wang, Rongzheng Wan, Hangjun Lu, Yusong Tu, and Peng Xiu

Abstract The dynamics of water molecules confined in nanochannels is of great importance for designing novel molecular devices/machines/sensors, which have wide applications in nanotechnology, such as water desalination, chemical separation, sensing. In this chapter, inspired by the aquaporins, which are proteins embedded in the cell membrane that regulate the flow of water but stop the protons, we will discuss the mechanism of water channel gating and water channel pumping, where water molecules form single-filed structure. The single-filed water molecules can also serve as molecular devices for signal transmission, conversion, and multiplication. Moreover, the water in the channel may have great potential applications in designing the lab-in-tube to controllable manipulation of biomolecules.

1.1 Introduction

With the development of nanoscience and nanotechnologies, particularly the successful fabrications of various nanochannels, the study of the water permeation across the nanoscale channels has become conceivable. The understanding of the

H. Fang (✉) • C. Wang • R. Wan
Shanghai Institute of Applied Physics, Chinese Academy of Sciences,
No.2019 Baojia Road, P.O. Box 800-204, Shanghai, 201800 China
e-mail: fanghaiping@sinap.ac.cn; wangchunlei@sinap.ac.cn; wanrongzheng@sinap.ac.cn

H. Lu
Department of Physics, Zhejiang Normanl University, Jinhua, 321004 China
e-mail: zjlhjun@zjnu.cn

Y. Tu
Institute of Systems Biology, Shanghai University, Shanghai, 200444 China
e-mail: tuyusong@gmail.com

P. Xiu
Bio-X Lab, Department of Physics, Zhejiang University, Hangzhou, 310027 China
e-mail: meihuazhuang@163.com

X.Y. Liu (ed.), *Bioinspiration: From Nano to Micro Scales*, Biological and Medical Physics, Biomedical Engineering, DOI 10.1007/978-1-4614-5372-7_1,

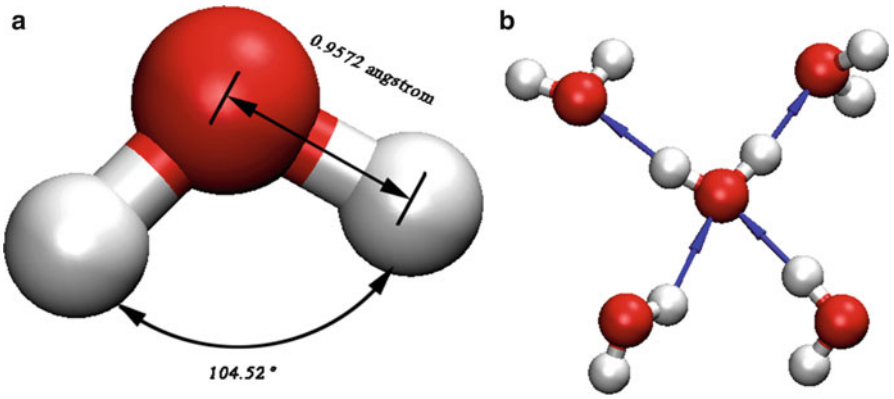

Fig. 1.1 (**a**) A water molecule, where the *red* and *gray balls* represent one oxygen atom and two hydrogen atoms. (**b**) A water molecule together with four neighboring water molecules. The *arrows* denote a hydrogen bond and the head and the end of an *arrow* shows the acceptor and the donor, respectively

dynamics of water molecules confined in nanochannels is also of great importance in designing novel molecular devices/machines/sensors, which have wide applications in nanotechnology [1–19], including lab-on-a-chip technology [20]. In this decade, the lack of clean water, particularly in developing countries, has become one of the main challenges. The desalination of seawater and filtration of polluted water [5] are regarded as two main methods to solve the clean water shortage. Considering the difficulty in the existing techniques, the nanotechnologies based on the water permeation across the nanochannels have become the most promising direction.

There have been many discussions on the water across the nanochannels [17, 21–28]. In 2001, Hummer et al., using molecular dynamics (MD) simulations, showed that water confined in very narrow nanochannels with appropriate radii displayed single-filed structure [21]. Later, Holt et al. [6] experimentally found that the water flow rate through a carbon nanotube (CNT) with a radius of 1–2 nm, a comparable radius to the CNTs used by Hummer et al. in the numerical simulations, was more than three orders of magnitude faster than the conventional nonslip hydrodynamic flow.

Biological systems always inspire us with new idea. In 1980s, Peter Agre discovered the aquaporins, which are proteins embedded in the cell membrane that regulate the flow of water but stop the protons [29, 30]. Later, the structure, the function, and the physics of aquaporins have been extensively studied both from experiments and from numerical simulations [31–39]. In 2001, Groot and Grubmuller used MD simulations to study the water permeation across the biological membrane proteins: aquaporin-1 (AQP1) and Glpf [32]. They found that the water molecules in those biological channels were single-filed. Later, Tajkhorshid et al. examined the apparently paradoxical property, facilitation of efficient permeation of water while excluding protons [34]. We note that people usually take the biological systems as

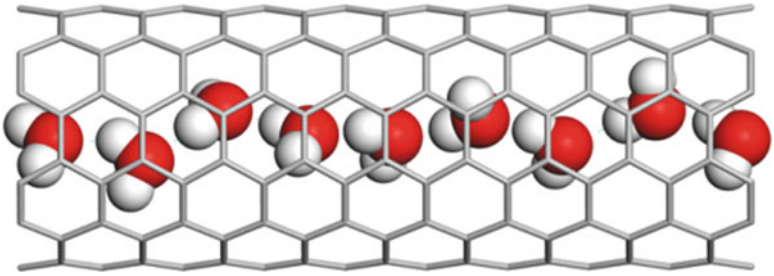

Fig. 1.2 A snapshot of water confined in a (6,6) armchair single-walled carbon nanotube. The *red* and *gray balls* represent the oxygen and hydrogen atoms, respectively. It can be seen clearly that each oxygen atom is located in the right side of the two hydrogen atoms in the same water molecule. The single-walled carbon nanotube is represented by *gray lines*

the most effective ones and can effectively shield the thermal noise and represent the useful signal. In this chapter, we will review the recent progress obtained by our group using MD simulations in the study of the water permeation across the nanoscale channels inspired by the aquaporins.

Let us first review the basic properties of water in a classical view. As is shown in Fig. 1.1, a water molecule is composed of one oxygen atom and two hydrogen atoms with the angle between OHO of about 104.52°. The water molecule is polar due to the residual charges on the oxygen atom and the hydrogen atoms. The most important thing in the water molecules is the hydrogen bonds between neighboring water molecules. Explicitly, an oxygen atom in one water molecule may have a strong interaction with a hydrogen atom in another, which is called the existence of a hydrogen bond. The strength of the hydrogen bonds, though much smaller than that of the chemical bonds, can be more than tens of $k_B T$. Thus, this bond usually plays a very important role in the system full of thermal fluctuation. It is believed that the anomalies of water mainly result from the existence of the hydrogen bonds.

1.1.1 Gating and Pumping of Nanoscale Channels

The water molecules are connected by one-dimensional hydrogen bonds as shown in Fig. 1.2 when the water molecules exhibit single-filed structure in a nanochannel. The motions of the water molecules are concerted transport through the channels. Obviously, at least one hydrogen bond should be broken if we want to stop the water flow across the nanotube. There are at least two methods to achieve this goal. One is to deform the nanotube and the other is to use external electric field to attract the water molecules.

As the model shown in Fig. 1.3, a single-walled carbon nanotube (SWNT) 13.4 Å in length and 8.1 Å in diameter is embedded in a graphite sheet as a water channel. The SWNT and the graphite are solvated in a box ($3 \times 3 \times 4$ nm) with water

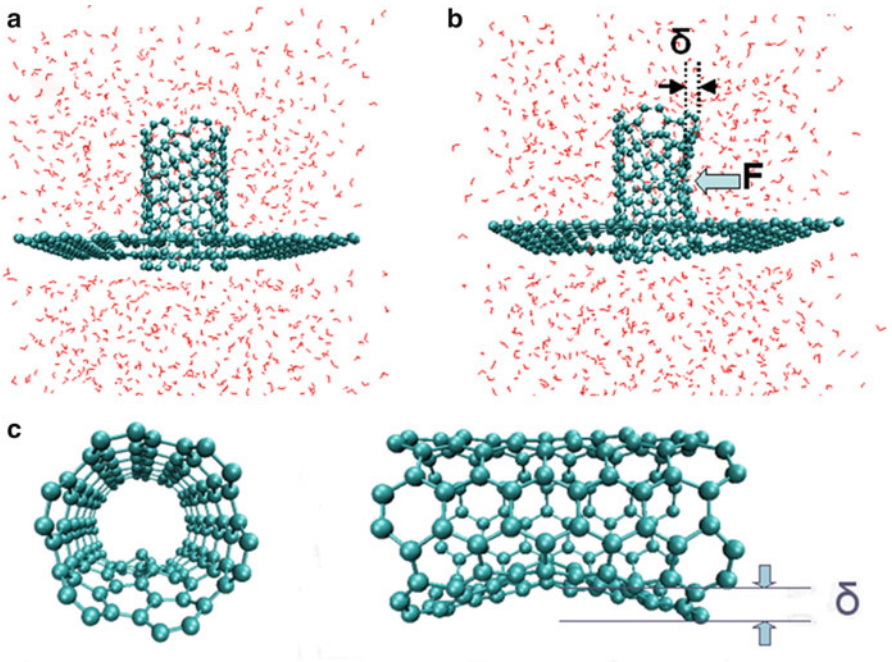

Fig. 1.3 (**a**, **b**) A snapshot of the simulation system. The single-walled carbon nanotube and the graphite sheet are solvated in a box ($3 \times 3 \times 4$ nm) with water molecules. The gap between the graphite plane and the nanotube is too small for a water molecule to penetrate. An external force, marked by "F," acts on an atom of the carbon nanotube and a deformation can be clearly seen (reprinted from [40]. Copyright 2005 American Chemical Society). (**c**) δ is the displacement of the atom directly acted by the external force from its initial equilibrium position

molecules using TIP3P water model. The SWNT can be controllably deformed by an external force F applied to one carbon atom (namely, the forced atom) in the right side of the CNT while the carbon atoms in the left half of the CNT were fixed [40]. In reality, the force can be the active force to control the flow or the perturbations from the other parts in the biological systems.

An additional acceleration of 0.1 nm ps^{-2} along the $+z$ direction is added at each atom to mimic an osmotic pressure difference of 133 MPa between two ends of the SWNT [23, 40]. The carbon atoms at the inlet, outlet, and where the external force is exerted are fixed to prevent the SWNT from being swept away in the simulation. The simulation is carried out at a constant pressure (1 bar) and temperature (300 K).

For each δ corresponding to an external force F, the time for the numerical simulation is 232 ns. The last 216 ns of the simulation are collected for analysis. Figure 1.4 displays the average number of water molecules inside the tube N, together with the net water flux averaged each 18 ns, as a function of time for each δ. For the unperturbed nanotube, the average number of water molecules inside the tube is about 5. During the entire 216 ns simulation, 1955 and 726 water molecules

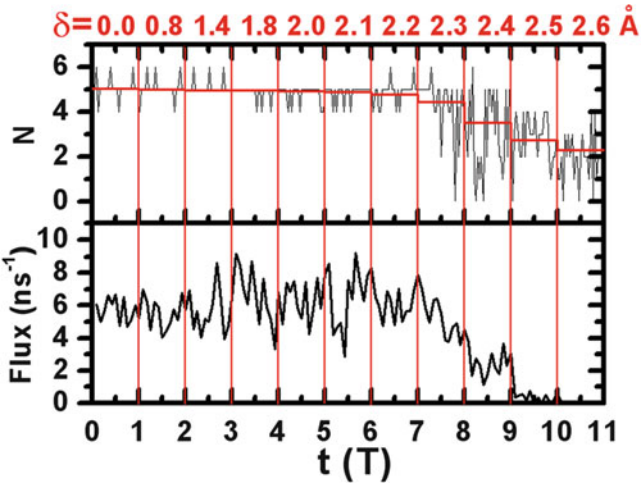

Fig. 1.4 Number of water molecules inside the nanotube (N) and the water flux (which is defined as the number of water molecules passing through the nanotube along z axis and the opposite direction per nanosecond) as a function of time for each deformation δ. The time period for each deformation δ is T, where $T = 12$ ns for N and 216 ns for the flux. The flux shown is averaged each 18 ns (reprinted from [40]. Copyright 2005 American Chemical Society)

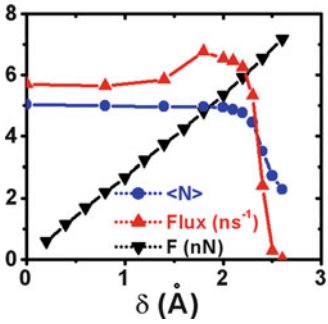

Fig. 1.5 Average number of N and the average net flux in the whole period of T, together with the force F acting on the atom, as a function of δ (reprinted from [40]. Copyright 2005 American Chemical Society)

pass through the tube along z axis and the opposite direction, respectively, resulting in a net water flux of 5.69 water molecules per nanosecond along z axis.

In macroscopy, as the force $F(t)$ increases, the flow across the nanotube decreases monotonically due to the increase in the deformation [40], which can be characterized by a parameter δ, which is the displacement of the forced-atom from its initial position in the pristine SWNT as shown in Fig. 1.3. However, in this system, the water flux and occupancy N do not decrease as expected as shown in Figs. 1.4 and 1.5 when δ increases from 0 to 2.0 Å. In the interval of 1.4 Å $< \delta < \delta_C \approx 2.0$ Å, the water flux even increases a little. Please be noted that the radius of a water molecule is only 1.4 Å. This shows that the water flux is unexpectedly stable even when the deformation of the forced-atom is larger than the

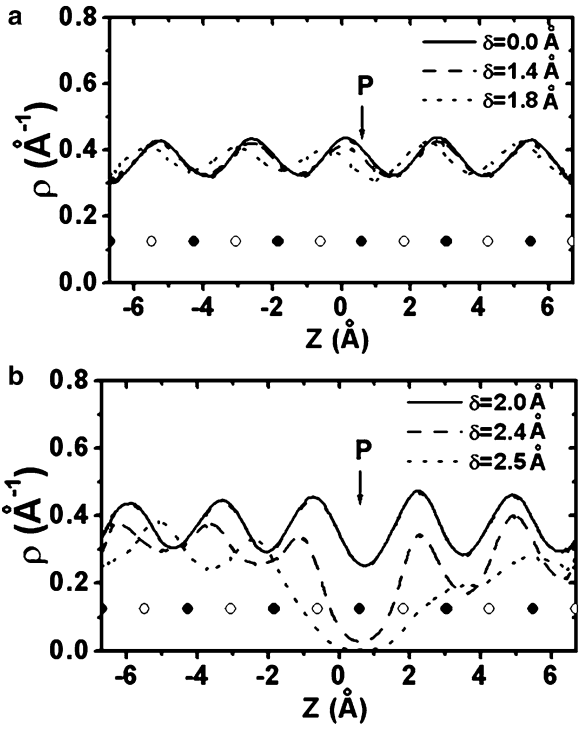

Fig. 1.6 Water distributions along z axis together with the positions of carbon atoms (the *open circles* and the *filled circles*). The *arrow*, marked by *P*, is the position of forced-atom. (**a**) $\delta = 0.0$, 1.4, 1.8 Å (**b**) $\delta = 2.0$, 2.4, 2.5 Å

radius of a water atom. Only when $\delta > \delta_C \approx 2.0$ Å, the net flux and the occupancy N decrease as δ further increases. When $\delta = 2.6$ Å, the water flux through the tube becomes a negligible value. In the total 216 ns simulation, no water molecules enter the tube from one end or leave from the other, indicating that at $\delta = 2.6$ Å, the nanotube is functionally closed. It shows that a CNT can be completely closed from an open state by moving the forced-atom by only 0.6 Å. Here, the CNT shows excellent gating behavior corresponding to external mechanical signals. On one hand, the water flux and occupancy of the CNT are extremely irrespective of external signals ($\delta < 2.0$ Å), for example, deformations due to noise. On the other hand, the water flux and occupancy of the nanotube are sensitive to further deformations. An additional increase of 0.6 Å for δ leads to an abrupt transition from an open state (flux same as an unperturbed nanotube) to a closed state (no flux).

In order to further study the physics for such gating behavior, we show the water distribution inside the CNT for different δ in Fig. 1.6. As is well known, the density of water is constant along a macroscopic channel with a uniform radius. However, for a CNT with 8.1 Å in diameter and 13.4 Å in length, the water density distribution appears in wavelike pattern. Furthermore, the gating of the water transportation through the CNT is found related to the wavelike pattern of water density distribution.

The water density distribution along the tube axis $\rho(z)$ can be calculated by

$$\rho(z) = \frac{N(z)}{N\Delta L},$$

where ΔL is the bin length and $N(z)$ is the number of water molecules appearing at the bin at z for the total of N snapshots from simulation. In order to compute the water density distribution near two openings of the CNT, we can extend the CNT from each end to bulk by 11.3 Å to construct a virtual cylinder with 8.1 Å in diameter. The whole cylinder was divided into 1,000 bins. In the case of $\delta = 0$ Å, the distribution has a wavelike structure with minimal values at the openings and five peaks, which is consistent with the average value of the water occupancy N ($N \approx 5$ for $\delta = 0$ Å from Fig. 1.5). For $0 \leq \delta < 2.0$ Å, the distribution changes gradually and the peak move leftward as δ increases, but the values of the peaks do not change much. This is conforming to the stable value of water occupancy N at the range of $0 \leq \delta < 2.0$ Å in Fig. 1.5. The water distribution at P, the location facing the forced-atom, decreases corresponding to the narrowing of the nanotube at P. When $\delta \geq 2.0$ Å, the distribution at P is smaller than that of the other dips, and the wavelike pattern is considerably deformed; the values of the peaks decrease obviously corresponding to the decrease in N in Fig. 1.5 at the same range of δ. The distribution at P is very close to zero when $\delta = 2.5$ Å. However, we still observe that about one water molecule enters from one side and leaves from the other side per nanosecond when $\delta = 2.5$ Å. Further inspection of the data shows that water molecules can pass the position of P very rapidly without staying.

The gating behavior can also be understood from the distance between the two water molecules, one left to the forced-atom and the other right to the forced-atom. As shown in Fig. 1.7, the distance almost keep the initial value without the deformation of the SWNT of 2–2.8 Å for $\delta < 2.0$ Å. Further increase in δ makes the distance increases rapidly, breaking the connection (hydrogen bonding) between those two water molecules. It is just the strong interaction of the hydrogen bonds that keeps the distance almost as a constant when $\delta < 2.0$ Å. Thus the water transportation across the nanotube stops.

As we have mentioned before, the water molecules form hydrogen bonds with neighboring water molecules, and the water molecules inside the CNT form a single hydrogen-bonded chain. The dipoles of the water molecules are nearly aligned along the nanotube axis. Due to the deformation of the nanotube, the total number of hydrogen bonds inside the nanotube decreases as δ increases (Fig. 1.8). The average number of the hydrogen bonds, denoted by N_{Hbond}, decreases very slowly in a linear fashion as $N_{\text{Hbond}} = 3.16–0.136$ Å in the range of $\delta < 2.0$ Å. In the range of $2.0 \text{ Å} \leq \delta < 2.5$ Å, N_{Hbond} decreases sharply from 2.87 to 1.43. This sharp decrease results from the decrease in the total water molecules inside the nanotube N as well as the increase in the distance between those two water molecules neighbor to the position P. The linear decrease in N_{Hbond} in the range of $\delta < 2.0$ Å mainly results from the increase in the distance between those two water molecules neighbor to the position P, for the value of N keeps stable in this range. The effect of the increase

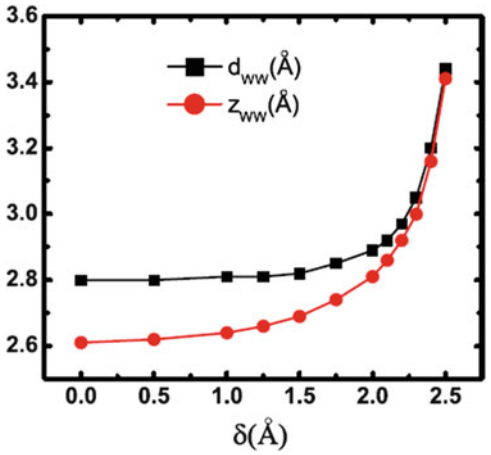

Fig. 1.7 The distance between the two water molecules near the forced-atom d_{WW} and its z-projection Z_{WW} for different δ (reprinted from [129]. Copyright 2008 American Physical Society)

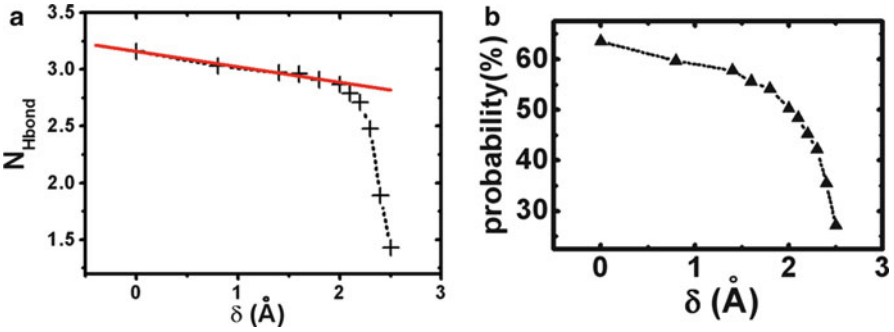

Fig. 1.8 (**a**) Average number of the hydrogen bonds inside the nanotube, the *solid line*, is a linear fit when $\delta < 2.0$ Å, and (**b**) the probability of the hydrogen bond formed by those two water molecules neighboring the forced-atom for different δ (reprinted from [40]. Copyright 2005 American Chemical Society)

in distance between two water molecules near P can be shown by the probability of the hydrogen bond formed by those two water molecules neighboring the forced-atom (Fig. 1.8). In the range of $\delta < 2.0$ Å, the deformation is not strong enough to perturb the hydrogen bonds chain inside the CNT, and the dynamics of water inside the CNT (e.g., occupancy and net flux) keeps stable in this range. When $\delta \geq 2.0$ Å, the deformation is strong enough to break the hydrogen bonds chain, resulting in a sharp decrease in water occupancy and net flux.

To explore the flipping behavior of water dipoles inside the CNT and its sensitivity to the deformation, we define ϕ as the angle between a water dipole and the nanotube axis, and $\bar{\phi}$ as the average angle of all the water molecules inside the tube. Some $\bar{\phi}$ for different δ are shown in Fig. 1.9. For the unperturbed CNT, $\bar{\phi}$ falls in two ranges $15^\circ < \bar{\phi} < 50^\circ$ and $130^\circ < \bar{\phi} < 165^\circ$ most of the time, which is

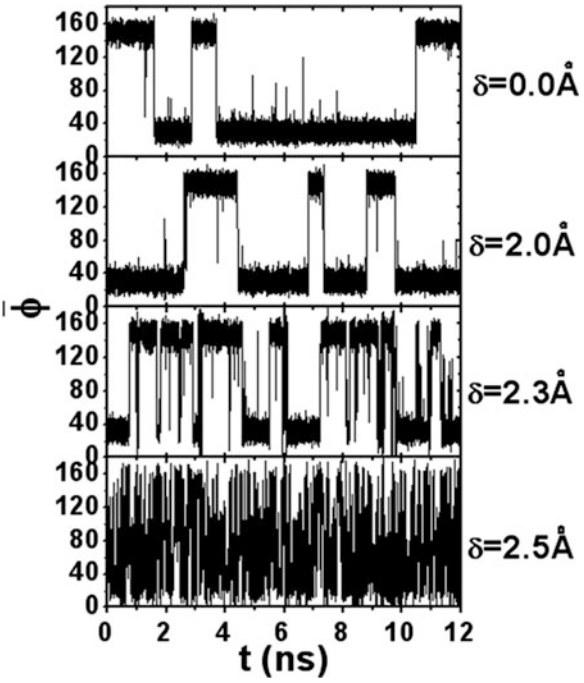

Fig. 1.9 $\bar{\phi}$ for $\delta = 0.0$, 2.0, 2.3, and 2.5 Å (reprinted from [40]. Copyright 2005 American Chemical Society)

consistent with the observation that the water molecules in CNT are nearly aligned. If we define a flip as $\bar{\phi}$ passing through 90°, we can calculate the number of flips per nanosecond, denoted by the flipping frequency f_{flip}.

The flipping frequency f_{flip} is governed by the potential barrier against flipping. And the increment of δ leads to two aspects of the potential change, decrease due to the breakage of hydrogen bonds inside the nanotube and increase due to the narrowing of the nanotube that confines water molecules to a smaller space. As is shown in Fig. 1.8, N_{Hbond} decreases very slowly with respect to δ for $\delta \leq 1.4$ Å. The confinement of water molecules is the main reason for the slow decrease in f_{flip} in this range.

As δ further increases, f_{flip} increases. The dependence of f_{flip} on N_{Hbond} is shown in Fig. 1.10. In the range of 2.0 Å $\leq \delta <$ 2.2 Å, the function

$$f_{\text{flip}} \propto \exp(-N_{\text{Hbond}} E_{\text{Hbond}}/kT)$$

can fit the data quite well, where E_{Hbond} is the average energy of a hydrogen bond in the nanotube for $\delta = 2.0$, 2.1, and 2.2 Å. Numerically, we find $E_{\text{Hbond}} = 12.96\,kT$. This exponential decay indicates that the change of the potential barrier mainly results from the decrease in the number of hydrogen bonds inside the nanotube in this parameter range. For even larger δ, say 2.5 Å, the water chain is frequently ruptured (Fig. 1.11). Only for a small period of time, $\bar{\phi}$ falls into the two parameter

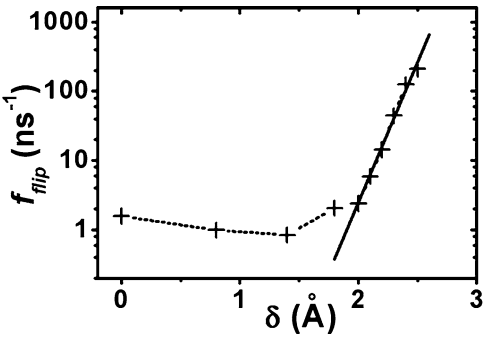

Fig. 1.10 Dependence of flipping frequency f_{flip} on the number of hydrogen bonds N_{Hbond}; the *solid line* is the fits for the exponential decay vs. N_{Hbond} (reprinted from [40]. Copyright 2005 American Chemical Society)

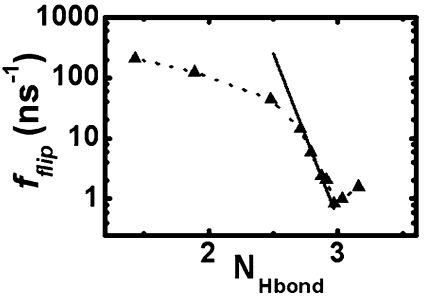

Fig. 1.11 Dependence of flipping frequency f_{flip} on δ. The *solid line* is the fit for the exponential growth vs. δ (reprinted from [40]. Copyright 2005 American Chemical Society)

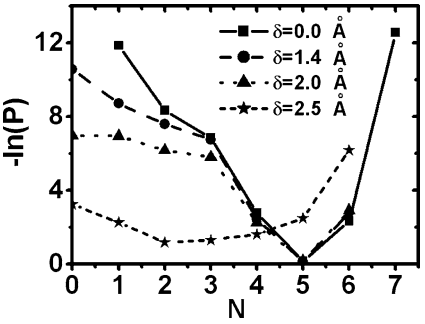

Fig. 1.12 Relative free energy depends on water occupancy, $\beta F(N) = -\ln p(N)$, for $\delta = 0.0$, 1.4, 2.0, and 2.5 Å (reprinted from [40]. Copyright 2005 American Chemical Society)

ranges, i.e., $15° < \bar{\phi} < 50°$ and $130° < \bar{\phi} < 165°$. However, in the interval of 2.0 Å $\leq \delta < 2.5$ Å, the exponential function $f_{\text{flip}} \propto \exp(\{\delta\}/\{\tau\})$ with $\tau = 0.107$ can fit the data very well (Fig. 1.11).

In order to show the water occupancy fluctuations, the free energy depends on water occupancy N as shown in Fig. 1.12. This relative free energy can be calculated by $\beta F(N) = -\ln p(N)$, where $p(N)$ is the probability of finding exactly N water molecules inside the nanotube. To obtain good statistics, data are collected every 0.25 ps in the calculation of $p(N)$. An approximate Gaussian occupation fluctuation is found for $\delta = 0$. The free energies for $\delta = 1.4$ Å and 2.0 Å are similar to those for $\delta = 0$. However, three events have been found with $N = 7$ for $\delta = 0$ while none

for $\delta = 1.4$ Å and 2.0 Å. And for the case of $N = 0$, it occurs 11 and 388 times for $\delta = 1.4$ Å and 2.0 Å, but none for $\delta = 0$. It seems that the effect of the deformation for $\delta \leq 2.0$ Å is considerable for the possibilities of the rare events although the change of the average value of the water molecules inside is negligible.

For $\delta = 2.5$ Å, the function of free energy is somewhat flat between $N = 2$ and 4, with a minimum at $N = 2$, due to the frequently rupture of the water chain. No intermittent filling is found in the range of $0 \leq \delta \leq 2.5$ Å, consistent with that there is not any minimum at $N = 0$. Although there are many cases with $N = 0$ for $\delta = 2.5$ Å, the durations for them are short. We have not found two successive data with $N = 0$, indicating that the duration for each case with $N = 0$ is less than 0.25 ps.

In addition, in MD simulations, the update algorithm develops a very slow change in the center of mass (COM) velocity, and thus in the total kinetic energy of the system, especially when temperature coupling is used. For the systems with limited friction, if such changes are not quenched, an appreciable COM motion will be developed eventually in long runs. Thus, the method of center of mass motion removal (CMMR) is necessary. During MD simulations, the CMMR method can be applied at a certain frequency. But for the systems with pressure difference to evoke a unidirectional transportation, for example, the gating system we discussed before, the application of CMMR may reduce the effect of such equivalent pressure difference.

It is clear that this excellent gating behavior results from the one-dimensional hydrogen bonds between the neighboring water molecules, which shield the external perturbations. Thus the water permeation across the bio-mimicked nanochannel with single-filed water molecules inside the nanochannel is effectively resistant to mechanical noises and sensitive to available mechanical signals.

Further, we consider the effect of CNT length on the behavior of water molecules in the tube. The CNT we choose is 14.6 Å in length and 8.1 Å in diameter. Along the z direction, it is embedded in the center of a graphite sheet, which is similar with the system shown in Fig. 1.3. A force is also applied to one carbon atom, namely the forced-atom. Note that the number of carbon rings along the nanotube is 5.5, which is 0.5 ring longer than the CNT used in previous sections. Interestingly, our simulation results indicate that the wavelike pattern of water density distribution becomes much weaker when the length of the perfect CNT is increased to 14.6 Å (see Fig. 1.13). Especially, the wavelike pattern is quite flat near the center of the CNT for the unperturbed nanotube. Even near two openings of the CNT, the wavelike pattern is less obvious than that of the CNT that is 13.4 Å. The height between the first peak and the dip from the left opening of the CNT is only about 0.05 $Å^{-1}$, which is much smaller than the average value of 0.12 $Å^{-1}$ for the CNT of 13.4 Å.

The shape of the CNT plays a role in the structure of the water density distribution along tube axis as well. Simulation results indicate that the weak wavelike pattern of water density distribution becomes obvious and shifts slightly when the CNT is deformed by external force. For $\delta < 1.5$ Å, the amplitude of

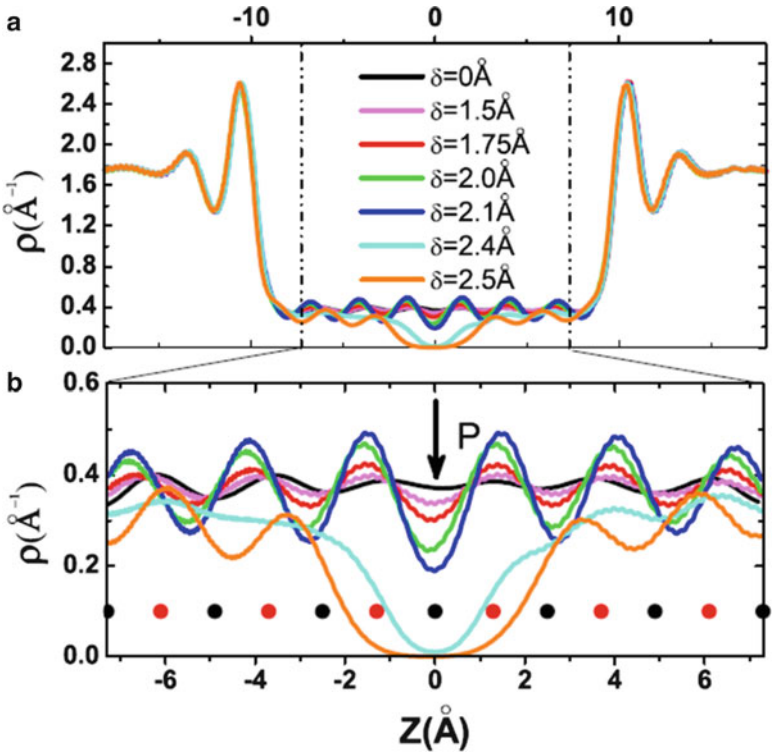

Fig. 1.13 (**a**) Water density distributions along z (carbon nanotube axis). (**b**) Water density distributions inside the nanotube together with the positions of the carbon atoms. The *red* and *black filledcircles* denote the positions of the carbon atoms. The *arrow*, marked by P, is the position of the atom affected by an external force (reprinted from [129]. Copyright 2008 American Physical Society)

wavelike pattern increases obviously, but the distances between crests and troughs change very little, almost fixed. For $1.5 < \delta \leqslant \delta_c \approx 2.0$ Å, the amplitude of the wavelike pattern increases sharply. From $\delta \approx 2.0$ Å and up, the wavelike pattern of the water density distribution was deformed and the density at P is smaller than that of the other parts. For $\delta \geqslant 2.5$ Å, the density distribution at P is very close to zero. Outside the CNT, the water density distribution is not affected by the shape of the CNT. There are two peaks near the two openings of the CNT due to the van der Waals (VDW) attraction of two graphite sheets.

The average number of water molecules inside the CNT of 13.4 Å is about five. For the CNT of 14.6 Å, the average number of water molecules inside the nanotube is about 5.5. The number of water molecules inside the CNT fluctuates with respect to time (see Fig. 1.14). There are two stable states with $N = 5$ and $N = 6$. The system switches mainly between the two states. The average durations for the states with

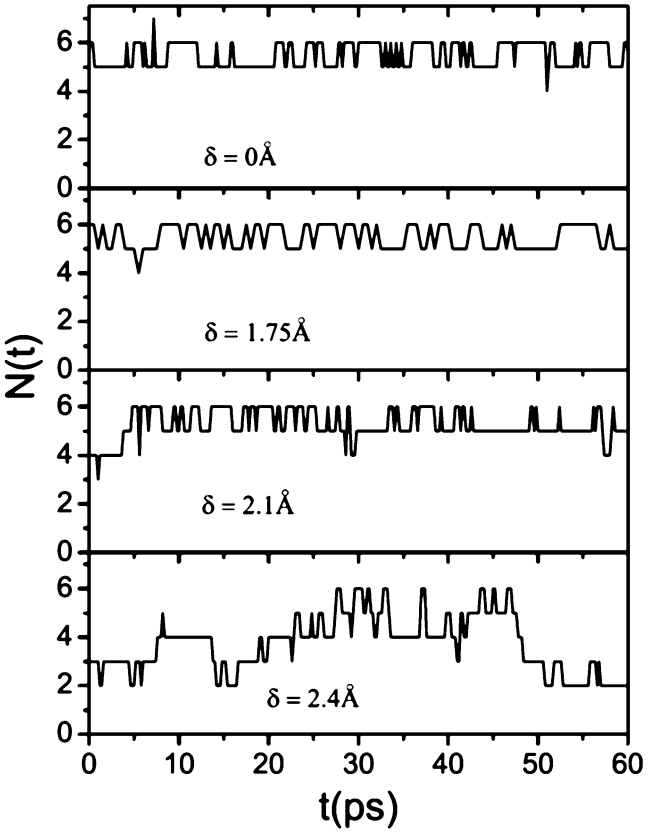

Fig. 1.14 Number of water molecules inside the carbon nanotube with respect to time in several representative systems (reprinted from [129]. Copyright 2008 American Physical Society)

$N = 5$ and $N = 6$ are 0.96 and 0.90 ps, respectively, showing similar probabilities for two states. When $\delta = 0$ Å, the total probabilities of $N = 5$, 6 are about 52 and 48%, both close to 50%.

The free energy of occupancy fluctuations $G(N)$ can be calculated by $G(N) = -k_B T \ln p(N)$, where $p(N)$ is the probability of N water molecules inside the nanotube, k_B is the Boltzmann constant, and T is the temperature.

Figure 1.15 shows that the free energy of $N = 5$ is close to the free energy of $N = 6$ for $\delta \leqslant \delta_c \approx 2.0$ Å. Profile of free energy of occupancy shows that two states of $N = 5$ and $N = 6$ are steady for $\delta \leqslant \delta_c \approx 2.0$ Å. The rapid transitions between the two states in the water permeation across the CNT are similar to those observed in the KcsA ion channel. However, for $\delta > \delta_c$, free energy of $N = 4$ is the minimum. The behavior of the single-filed water molecules inside the nanotube becomes different.

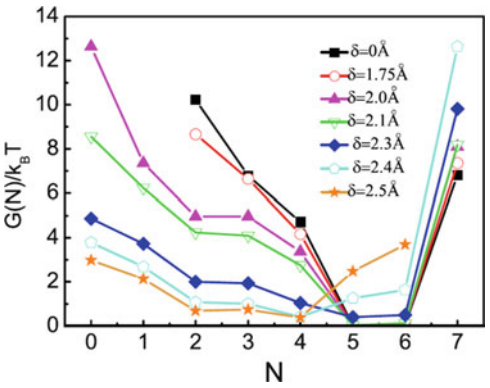

Fig. 1.15 Free energy of occupancy fluctuation for different δ (reprinted from [129]. Copyright 2008 American Physical Society)

Now, we consider the question why the water density distribution is so flat for the unperturbed nanochannel and the wavelike pattern becomes obvious as the CNT is deformed by external force.

For the unperturbed CNT with 14.6 Å in length, there are two steady states of $N = 5$ and $N = 6$. Their probabilities are both close to 50%. From Fig. 1.16, we can see that the water probability densities of $N = 5$ and $N = 6$ show obvious wavelike pattern. The average amplitude is about 0.32 $Å^{-1}$. The distance between troughs and crests of the waves is about 2.6 Å, close to the length of the hydrogen bonds between water molecules. However, the wave profiles of $N = 5$ and $N = 6$ are not in the same phase. The phase difference between them is about 1/2 period. Thus, the total water probability density becomes flat from the superposition of those two cases, especially in the middle region.

When the middle part of the CNT is pressed by the external force, the density distribution pattern changes correspondingly. It is noted that the crest of the water probability density of $N = 5$ just locates in the middle part of the CNT, while the corresponding position is the trough of the water probability density of $N = 6$. Thus, the wavelike pattern of $N = 6$ almost keeps the initial profile of $\delta = 0$ Å, while the amplitude of $N = 5$ becomes smaller. Thus, the flat profile of the total water density distribution is broken, showing a new wavelike pattern.

In the case of $\delta = 2.4$ Å, the middle portion of the CNT becomes narrower. There are clear valleys in the middle portion for all the cases of N, resulting in a big valley in the total water density distribution.

So now we know the reason why the total water density distribution in the middle part is flat and becomes wavelike pattern when the middle portion of the nanotube is narrowed. It results from the phase difference between the two states of $N = 5$ and $N = 6$, and the deformed portion just locates in the middle. But the origins of the wavelike pattern of water density distribution of $N = 5$ and $N = 6$ are still not clear.

First, we calculate the water–CNT interaction along the nanotube axis. The results are shown in Fig. 1.17.

"U"-like profile of water–CNT shows that the more middle water molecule locates in, the stronger the CNT attracts water molecules. When the middle portion

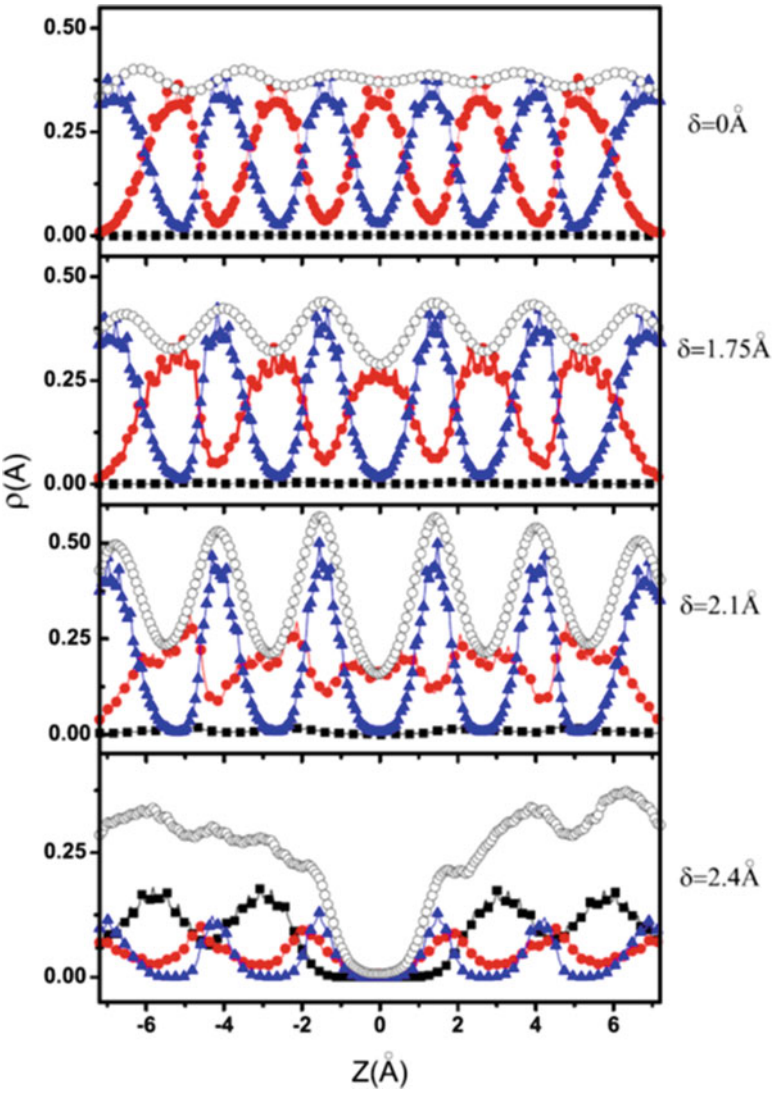

Fig. 1.16 Water probability density along the nanotube axis. *Black filledsquares* indicate the water probability density of $N = 4$, *red filledcircles* indicate the water probability density of $N = 5$, and the *open circles* indicate the total water probability density (reprinted from [129]. Copyright 2008 American Physical Society)

of the CNT is narrowed by the external force, the water–CNT interaction of a water molecule in the middle becomes positive. The profile changes from "U" shape to "W" shape. The deformed portion interrupts the single-filed water molecules inside the CNT.

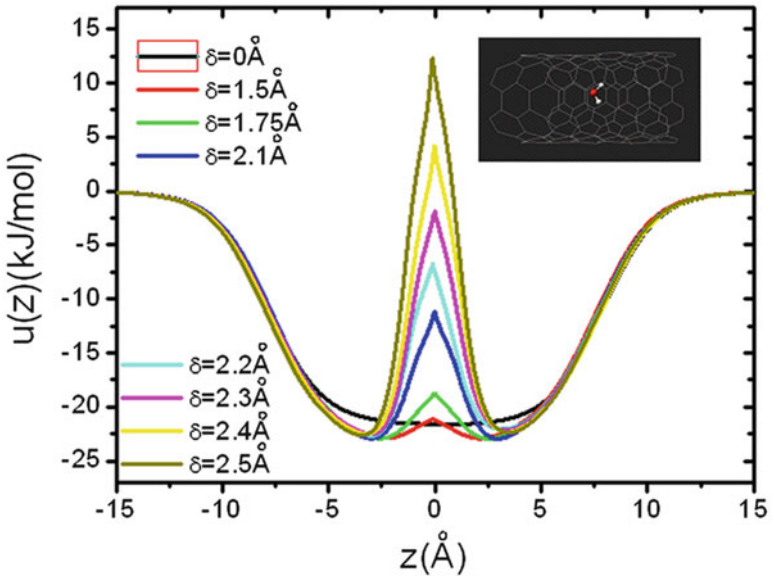

Fig. 1.17 Water–CNT interaction energy $u(z)$ of a water molecule at z with the carbon nanotube. The inset shows a water molecule locating in the center of the cross section at z of the carbon nanotube. Water–CNT interaction, $u(z)$, is calculated by $u(z) = 4\varepsilon_{CO} \sum_{i=1}^{i=156} \left[\left(\frac{\sigma_{CO}}{r_i} \right)^{12} - \left(\frac{\sigma_{CO}}{r_i} \right)^{6} \right]$, where r_i is the distance between the water molecule and ith carbon atom. In the calculation, we assume that the water molecule locates at the center of the cross section of the nanotube (reprinted from [129]. Copyright 2008 American Physical Society)

Now, we present a theoretical model to understand the origin of the wavelike pattern of water density along the nanotube axis. There are three assumptions:

1. Water molecules inside the nanotube form a single-filed chain.
2. The distance between any two neighboring water molecules inside the nanotube along the z direction is fixed, which is denoted by d.
3. The change in free energy of the single-filed water inside the nanotube mainly results from the change in water–CNT interaction energy $u(z)$ when the CNT is deformed by the external force. Water molecules inside the nanotube form a single-filed chain.

If we know the water–CNT interaction energy $u(z)$ and the distance between the two neighboring water molecules inside the CNT, according to the above three assumptions, we can calculate the water probability density along the CNT. Both the water–CNT interaction and the distance between the two neighboring water molecules can be obtained without numerical simulations. $u(z)$ is shown in Fig. 1.17. The equilibrium distance between the two water molecules is about 2.8 Å. Considering that the water molecules inside the channel are usually connected by

hydrogen bonds and appear in zigzag structure instead of a line (see Fig. 1.7), the distance between the two water molecules along the z direction is about 2.6 Å.

The total potential $U(z)$ of water molecules inside the CNT is given by

$$U(z) = \sum_{i=-\infty}^{i=+\infty} u(z + id) f(z_i), \tag{1.1}$$

where z is the coordinate of a water molecule (denoted by P_0). $i > 0$ indicates that the water molecule locates only in the right side of the $P_{0,}$ vice versa. $f(z_i)$ is a truncation function, which is given by

$$f(z_i) = \begin{cases} 1 \text{if} z_{\min} \leqslant z_i \leqslant z_{\max}, \\ 0 \text{if} z_i < z_{\min}, z_i > z_{\max}, \end{cases}$$

where $z_{\min}$ and $z_{\max}$ are the z-coordinates of the left and right ends of the CNT, respectively.

The probability density of finding water molecules at position z can be assumed as

$$\rho(z) = A \exp[-U(z)/k_B T], \tag{1.2}$$

where k_B is the Boltzmann constant, T is the temperature of the system, and A can be determined by the average number of water molecules in the CNT,

$$< N >= \int_{z_{\min}}^{z_{\max}} \rho(z) \mathrm{d}z. \tag{1.3}$$

According to (1.1) and (1.2), we can calculate the probability density of the representative systems.

Comparing between the theoretical results and the simulation results for $\delta = 0$ Å (see Fig. 1.18), we can find that the main structure of water probability density distribution is consistent. Similar to the simulation results, the curves of the theoretical result in the case of $N = 5$, 6 have five and six troughs, respectively. The peaks of the curves of the theoretical results are a little sharper than those of the simulation results, mainly results from that in the above model, the distance between water molecules inside the CNT is assumed to be a constant. In reality, the distance between neighboring water molecules fluctuates according to the interaction potential.

When the CNT is deformed by external force, the water–CNT interaction energy will increase correspondingly (see Fig. 1.17). According to (1.2), the probability of finding water molecules in the narrow portion of the CNT decreases. The deformation greatly changes the water density distribution especially for $N = 5$, while slightly for $N = 6$. The errors in the theoretical predictions increase with the deformation of CNT. The main reason is that the distance between neighboring

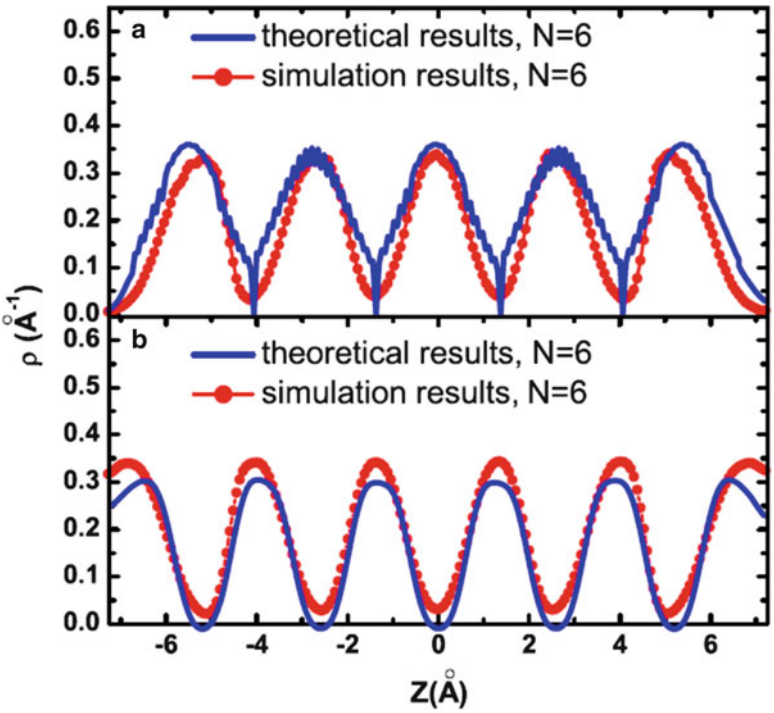

Fig. 1.18 The water probability density distributions along the nanotube axis for $\delta = 0$ Å (reprinted from [129]. Copyright 2008 American Physical Society)

water molecules located in the middle part of the nanotube increases. The distance between water molecules is not a constant in this case. But in the above model, d is assumed to be fixed. As δ further increases from δ_c, the error of the theoretical prediction increases very quickly (see Fig. 1.19).

From the theoretical model, we can understand the origin of the wavelike pattern of water density distribution inside the CNT. The wavelike pattern mainly results from the potential barriers at both ends of the nanotube together with the tight hydrogen-bonding chain inside the tube that fixes the distance between neighboring water molecules approximately.

We know, for molecular biological systems, that the external and internal fluctuations are usually nonnegligible. In this section, we will discuss the effect of the external fluctuation on water molecule transportation. Different from the above where the forced-atom is fixed, if the forced carbon atom vibrates periodically, the behavior of the single-filed water chain inside the CNT still keeps stable. The simulation framework is similar to the simulation system in Fig. 1.3. In this system, the forced-atom is forced to move according to the equation

$$x = x_0 + A\cos(\omega t + \phi),$$

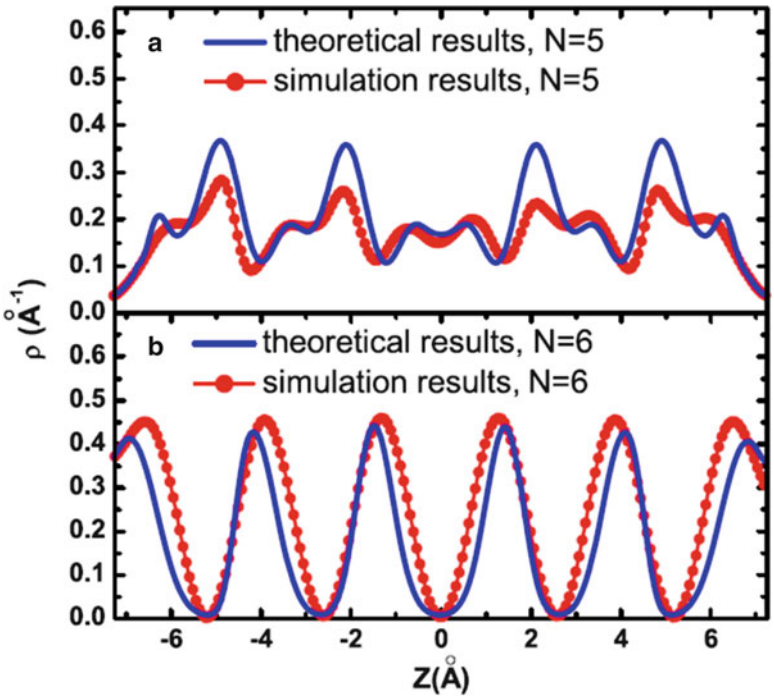

Fig. 1.19 The water probability density distributions along the nanotube axis for $\delta = 2.1$ Å (reprinted from [129]. Copyright 2008 American Physical Society)

where x_0 is the initial position of the vibrating carbon atom, A is the amplitude, ω is angular frequency, and ϕ is the initial phase. The frequency is defined as $\frac{\omega}{2\pi}$. It is found that the vibrating frequency, f, plays a role in water transportation through (6,6) CNT.

From the simulation result shown in Fig. 1.20, we can find that the water flow, net flux, and $<N>$ almost keep the value of the unperturbed system when the frequency $f < f_c \approx 1,333$ GHz. The corresponding period time is 0.75 ps and the velocity of the moving-atom under this frequency (f_c) is about 200 m/s, about half the average thermal velocity of water molecules (nearly 400 m/s) at room temperature. In real systems, it is impossible for a carbon atom in CNT to vibrate at such a high velocity and in such a large amplitude (2 Å). Thus, the permeation property of the water molecules confined in the nanochannel can be effectively shielded from strong noise.

From Fig. 1.21, we can find that the water density distribution maintains the similar wavelike pattern for $f < f_c \approx 1,333$, which leads to the invariability of the total number of water molecules inside the nanotube. The single-filed water chain connected with hydrogen bonds can accommodate the fluctuation of the CNT due to external force. For $f > f_c$, the wavelike pattern of density distribution is destroyed.

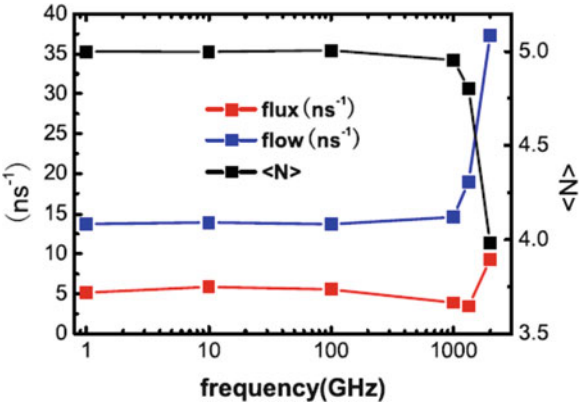

Fig. 1.20 Flux, flow, and average number of water molecules inside the CNT for different vibrating frequencies f (reprinted from [130]. Copyright 2008 Chinese Physics Society)

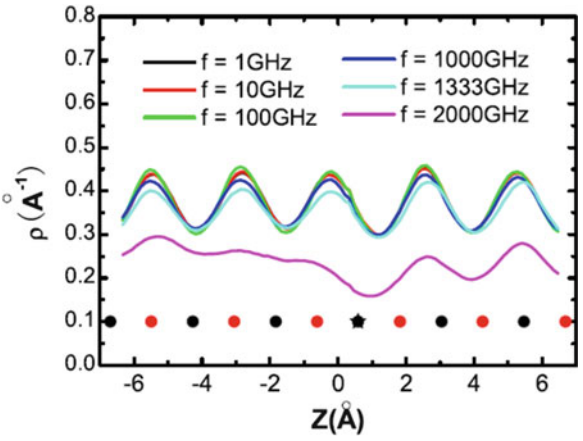

Fig. 1.21 Water density distribution along the nanotube axis. The *open* and *filled circles* denote the locations of the carbon atoms. The *asterisk* is the position of the vibrating atom affected by an external force (reprinted from [130]. Copyright 2008 Chinese Physics Society)

Fluctuations of CNT induce the number of water molecules inside the nanotube to decrease and the velocity of the transportation of water chain to increase.

Water molecules confined inside the (6,6) CNT form a single-filed chain connected by hydrogen bonds. An important feature of the hydrogen bond is that it possesses directionality (see Fig. 1.1). Molecular transport through the quasi-one-dimensional CNT is highly collective, since motion of one water molecule requires concomitant motion of all water molecules in the file. The chain rarely ruptures because of the tight hydrogen bonds in the protective environment of the CNT. Hydrogen bonds nearly align along the nanochannel axis and collectively flip in their orientations. The orientation of water chain is defined by a characteristic angle $\overline{\varphi}$ [40]. There are two stable states $15° < \overline{\varphi} < 50°$ and $130° < \overline{\varphi} < 165°$ and $\overline{\varphi}$ switches between them (see Fig. 1.22). Here we define a flip as $\overline{\varphi}$ transforms from one state to another state passing through $\overline{\varphi} = 90°$. During the flipping process, under the transition state, a hydrogen bond defect along the water chain inside the SWNT is formed. The flipping frequency f_{flip} for different vibrating frequency is shown in Fig. 1.23. Interestingly, the effect of the vibration of the CNT on the

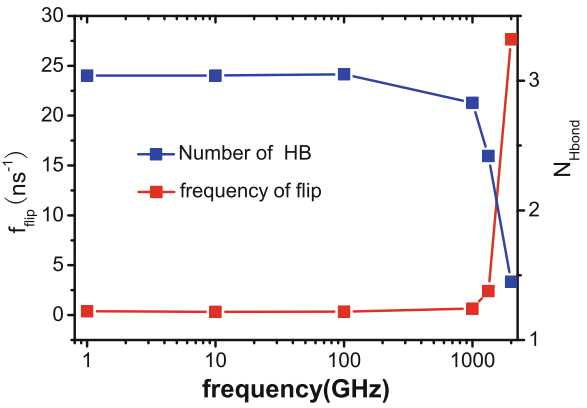

Fig. 1.22 Characteristic angle, $\overline{\varphi}$, for different vibrating frequency f (reprinted from [130]. Copyright 2008 Chinese Physics Society)

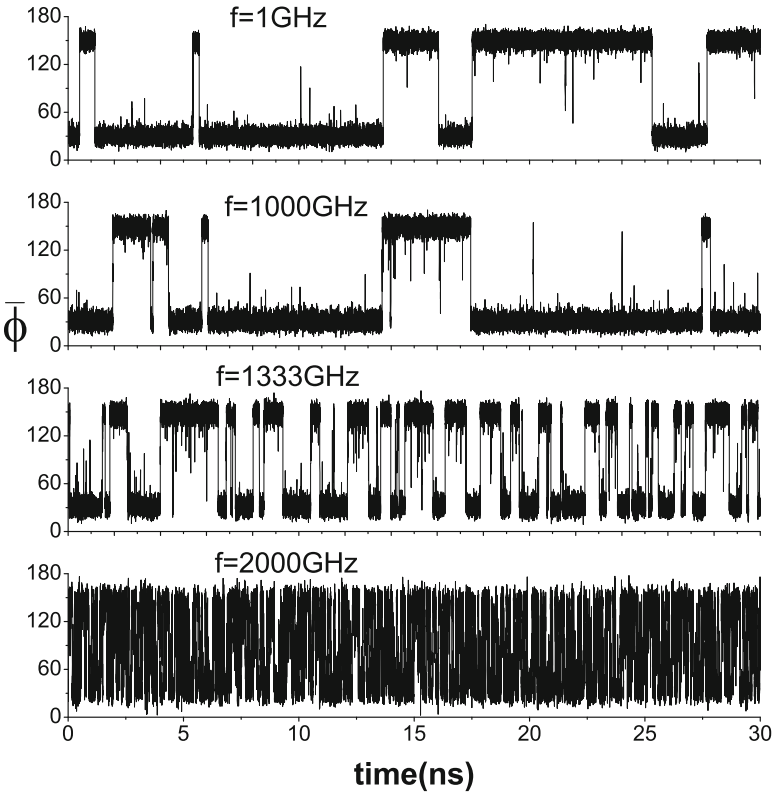

Fig. 1.23 Average number of the hydrogen bonds inside the nanotube and the flipping frequency for different vibrating frequency f (reprinted from [130]. Copyright 2008 Chinese Physics Society)

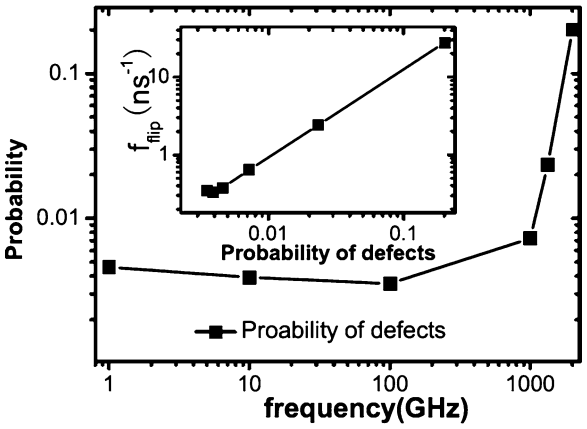

Fig. 1.24 Probabilities of defects vs. vibration frequency f and (inset) f_{flip} with respect to the probabilities of defects (reprinted from [130]. Copyright 2008 Chinese Physics Society)

frequency of flip is limited for $f < f_c$, which results from the stability of the whole water chain confined inside the CNT. As f becomes larger than f_c, the flipping frequency increases sharply. The hydrogen bond near the middle part of water chain is usually broken due to violently vibrating, which induces hydrogen bond defects in the middle portion of the CNT, not only in the inlets of the nanotube.

The dipole flip of ordered water chain inside the CNT is the process that a hydrogen-bonding defect moves through the tube. Figure 1.24 gives the probability of defects (corresponding to transition states) with respect to the vibrating frequency and the relationship between the dipole flipping frequency and the probability of defects. Similar to the above results, for $f < f_c$, the effect of the vibrating fluctuation on the formation of defects is slight. As frequency grows above f_c, the probability of defects increases dramatically. Correspondingly, the dipole flipping frequency increases sharply. From simulation results shown in the inset of Fig. 1.24, we find that the function $f_{\text{flip}} = f^0_{\text{flip}} + A * P$ can fit the data quite well, where P is the probability of defects in water chain, $f^0_{\text{flip}} = -0.36\text{ns}^{-1}$, and A is 139.47 ns^{-1}.

The above sections have discussed the effects of the geometrical shape on the transportation of water molecules through the nanochannels by deforming the CNT. Simulation results indicate that pressing the middle part of the CNT by external force can control the transportation of water chain well. Now we focus on discussing the effects of the position of the controllable region on water transportation.

The simulation framework is shown in Fig. 1.25. In order to explore the effect of the position of the narrow region on water transportation, one carbon atom (the forced-atom) is pushed away from its initial position, resulting in 2.2 Å radial displacement in each simulation system. Seven different systems are considered by choosing different forced-atoms (spheres of the nanotube shown in Fig. 1.25). For the convenience of analysis, the middle carbon atom is taken as the origin point of the z axis, and the distance between the forced-atoms and origin point is denoted by d. The positions of forced-atoms indexed from 1 to 7 are −7.4, −4.9, −2.5, 0, 2.5, 4.9 and 7.4Å, respectively.

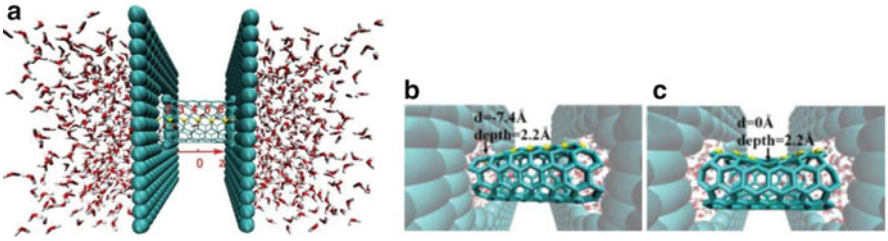

Fig. 1.25 Simulation framework. The spheres of the nanotube denote the possible forced-atoms and d is the z coordinate of the possible forced-atom (reprinted from [131]. Copyright 2011 American Physical Society)

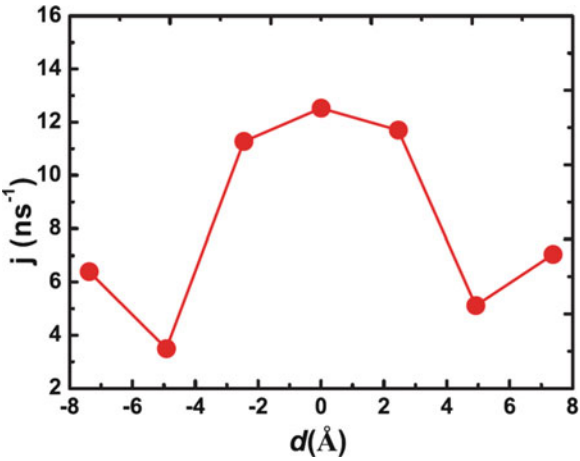

Fig. 1.26 The water flux across the carbon nanotube for different deformation positions d (reprinted from [131]. Copyright 2011 American Physical Society)

Our first observation is that the net water flux is sensitive to the position of the deformation (see Fig. 1.26). For the unperturbed CNT, the net water flux is about 14.8 ns^{-1}. The W-type profile shows that the water flux peaks at 12.5 ns^{-1} when the deformation exists in the middle region ($d = 0$ Å) of the SWNT. And it decreases sharply as long as the deformation position moves away from the middle region. Note that if the deformation position moves from $d = 0$ Å to $d = -4.9$ Å (~2.5 Å distance from the end of the nanotube), the net water flux reaches the minimum. One readily sees that the net water flux decreases dramatically when the deformation position occurs near the end of the SWNT. The flux for $d = -4.9$ Å falls to only approximately one quarter of the flux for $d = 0$ Å. In other words, the nozzle effect is very important for water permeation. Furthermore, simulation results indicate that the W-type profile is not fully symmetrical, even though the deformation positions are symmetrical at approximately $d = 0$ Å (see Figs. 1.25 and 1.26). For example, the net water flux for $d = -4.9$ Å (3.5 ns^{-1}) is obviously smaller than that for $d = 4.9$ Å (5.1 ns^{-1}). Meanwhile, the net water fluxes for $d = -7.4$ and 7.4 Å also exhibit similar behavior and their values are 6.4 and 7.0 ns^{-1}, respectively.

We now come to exploit the question why the location of the narrow portion plays a key role in water transportation through the nanotube. We have known that the transportation behavior of water molecules is mainly determined by the profile of the total interaction potential (it is denoted by the symbol P in this chapter). In this section, potential includes two parts: one is the water–water interactions (the interaction energies of the water molecule at position z inside the SWNT with its neighboring water molecules), denoted by P_{WW}, and the other part is the water–SWNT interactions (the interactions of the confined water at position z with the carbon atoms of SWNT), denoted by P_{WC}. It is consistent with the results shown in Fig. 1.17 that the potential energy curve of P_{WC} for the unperturbed SWNT has a symmetrical "U-like" shape, and the lowest is located in the middle of the SWNT (the position of $z = 0$ Å). When the SWNT is narrowed at d, the potential barrier appears at $z = d$. The profile of the curve of P_{WC} changes from a "U-like" shape into a "W-like" shape. As the location of the narrow portion moves to the ends of the nanotube, the peak of P_{WC} moves to the openings of the nanotube correspondingly, and the height of the peak increases due to a "U-like" shape of P_{WC} for the unperturbed SWNT.

Water molecules inside the CNT are connected by hydrogen bond. The strength of the energy is about $10\,k_BT$. For $|d| \leqslant 2.5$ Å, the hydrogen-bonding chain structure inside the SWNT is still perfect because the water–SWNT interaction potential P_{WC} is negligible compared to the strength of the hydrogen bond. However, if the location of the deformation moves out from the middle region, the water–SWNT interaction energy increases obviously. Thus, for $|d| \geqslant 4.9$ Å, the possibility of producing defects by breaking the hydrogen bond increases dramatically. Figure 1.27 shows that P_{WW} for $d = -4.9$ Å peaks at $z = -2.1$ Å, which is ~2.8 Å (about the size of a water molecule) away from the deformed position of $z = d = -4.9$ Å, indicating that the hydrogen bond that connects between the water molecule at $z = -2.1$ Å and its left one (the water molecule at $z = -4.9$ Å) usually is violated. Correspondingly, for $d = -4.9$ Å, the value of P_{WW} ($z = -4.9$ Å) is lower than that of P_{WW} ($z = -2.1$ Å). In fact, it results mainly from that the possibility of the water molecule located in $z = -2.1$ Å is larger than that in $z = -4.9$ Å due to P_{WC} ($z = -4.9$ Å) > P_{WC} (-2.1 Å). Certainly, the average number of the hydrogen bonds of the water molecule at $z = -2.1$ Å is larger than that of the water molecule at $z = -4.9$ Å. In other words, when there is a water molecule near $z = -4.9$ Å, usually there exist water molecules in two sides of it (near $z = -2.1$ Å and $z = -7.7$ Å), rather than vice versa. P_{WW} ($z < -4.9$ Å) is lower than P_{WW} ($z > -4.9$ Å) because the water molecules in the region of $z < -4.9$ Å are closer to the bulk water than those in the region of $z > -4.9$ Å. The same mechanism (water molecules near $z = -7.9$ Å are closer to the bulk water than those near $z = -4.9$ Å) makes the height of the peak of P_{WW} for $d = -7.4$ Å lower than that for $d = -4.9$ Å. The total interaction potential $P(z)$ is given by $P(z) = P_{WC}(z) + P_{WW}(z)$. For $d = -7.4$, -4.9, 4.9, and 7.4 Å, the distributions of $P(z)$ are lifted up. The higher the total interaction potential is, the less the water flux through the CNT is. In the case of $d = 0$ Å, the average interaction potential is lower than that in the others, which results in the largest net flux. In the cases of $d = -4.9$

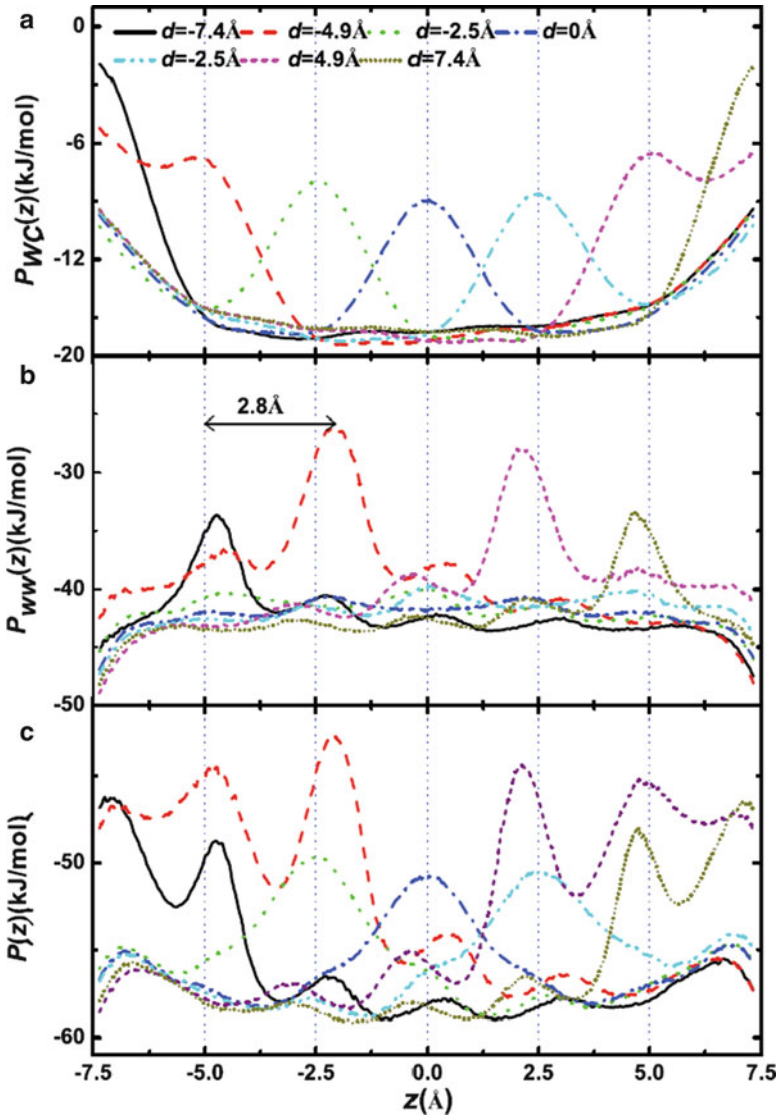

Fig. 1.27 The average water–SWNT interaction energy, water–water interaction energy, and the total interaction energy along z for different d (reprinted from [131]. Copyright 2011 American Physical Society)

and 4.9 Å, the average interaction potentials are large. Correspondingly, the net water flux in these two systems is small. The net water flux is mainly regulated by the water–water interaction and water–carbon interaction. The different position of the narrow region results in a change of the total interaction potential, meanwhile the net water flux changes.

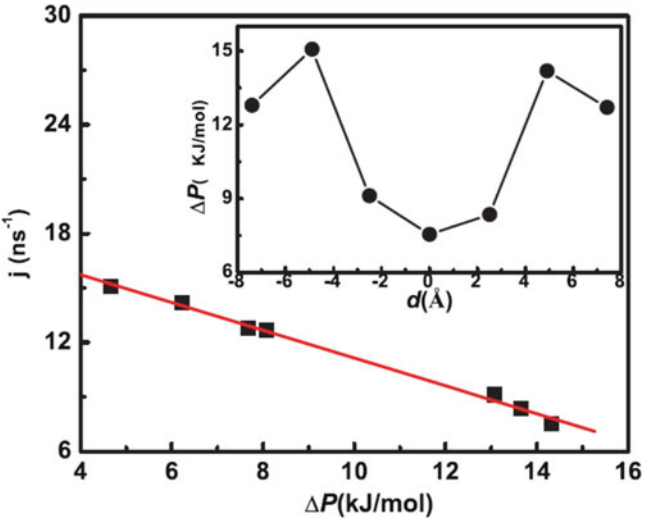

Fig. 1.28 The water flux j for different ΔP and (inset) ΔP for different d. In this figure, ΔP is the difference between the maximum and the minimum of the interaction potential, which is usually used to characterize the potential profiles (reprinted from [131]. Copyright 2011 American Physical Society)

From Fig. 1.28, we can find the M-type profile of ΔP, showing that ΔP approaches to the minimum as the narrow portion moves to the middle of the SWNT. The corresponding value of ΔP is $\sim$7.7 kJ mol^{-1}, only half of the ΔP for $d = -4.9$ or 4.9 Å. Consequently, the flux for $d = 0$ Å approaches to the maximum. From the simulation results shown in Fig. 1.28, we can find that the water flux decreases almost linearly with increasing ΔP. The data can be well fitted by the following formula:

$$j = j_0(1 - \Delta P/\varepsilon),$$

where $\varepsilon \approx 18.1$ kJ mol^{-1} and $j_0 = 21.7$ ns^{-1}. According to the above fitted formula, the net water flux would decrease to zero when $\Delta P = \varepsilon \approx 18.1$kJ mol^{-1}. To check the validity of the prediction, a system of depth = 2.3 Å and $d = -4.9$ Å was simulated, and then the simulation result shows that the net water flux is still $\sim$0.6 ns^{-1} and the matching ΔP is $\sim$22 kJ mol^{-1}, implying that the fitted linear law is a good fit only for $\Delta P < 16$kJmol^{-1}.

From the above simulation results and discussions, it is concluded that the water flux is not only sensitive to the strength of the deformation but also significantly influenced by the location of the deformation. When the deformation is just located in the middle of the nanotube, forming an hourglass-shaped region, the water flux across the nanotube reaches a maximum. Simulation results furthermore indicate that the hourglass shape is more convenient for water molecules to pass through the nanotube than a funnel shape.

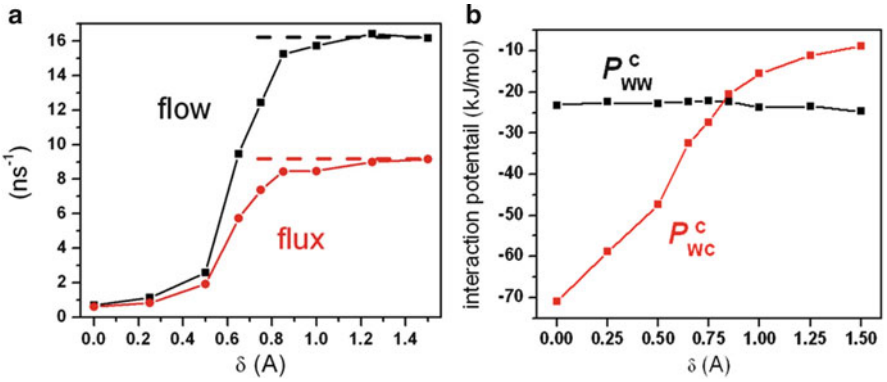

Fig. 1.29 (**a**) Averaged water flow (*black*) and net flux (*red*) through the channel with respect to δ, together with those for the system without an external charge (*dashed lines*). δ is the distance of the imposed charge to the centerline minus the radius of the single-walled carbon nanotube. (**b**) Values of P^{C}_{WC} and P^{C}_{WW}, with respect to δ. P^{C}_{WC} is the electrostatic potential between the water molecule in the middle of the nanotube with the imposed charge, and P^{C}_{WW} is the average value of the electrostatic potential between the water molecule and one of its neighboring water molecule (reprinted from [22]. Copyright 2007 National Academy of Science, USA)

Electrical field can also be used to control the channels. Electrical field can be initiated by an external charge. As is shown in Fig. 1.29, we have introduced a positive charge of quantity $1.0e$ on the plane of the graphite that divides the full space into two parts [22]. Similar to the case under the deformation of the SWNT, the average flow and net flux across the channel are approximately equal to those in the system without any charge until a value of $\delta_C = 0.85$ Å. Here, the distance of the imposed charge to the centerline minus the radius of the SWNT is also denoted by δ. Both the average flow and net flux decrease monotonically and sharply as δ further decreases. At $\delta = 0$, the channel is almost closed with the average flow below 1.0 ns^{-1}.

These behaviors result from the competitions between the water–charge interaction and the water–water interaction (mainly from the hydrogen bonds). As is shown in Fig. 1.2, all the water molecules inside the channel have orientation concerted, along or opposite to the nanotube. This orientation distribution is not easy to be changed by an external charge outside the nanotube due to the strong hydrogen bonds between the neighboring bonds. Only when the charge is close enough so that the interaction of the water and the charge is comparable to a hydrogen bond, the water chain inside the nanotube shows considerable change. In Fig. 1.29, we show the average value of the electrostatic potential between the water molecule in the middle of the nanotube with the imposed charge, P^{C}_{WC}, together with the average value of the electrostatic potential between the water molecule and one of its neighboring water molecule. It is clear that at $\delta \approx \delta_C$, $P^{C}_{WW} = P^{C}_{WC}$. Further approach of the charge makes the interaction between the water and the charge stronger, and the orientation of the water molecule facing the charge changes its

direction, becoming to point to the external charge, which makes the interaction between the water and the charge even stronger. This will result in more difficulties when water molecules move along the nanotube, thus the net flux across the nanochannel decreases.

It seems that the water permeation across the bio-mimicked nanochannel with single-filed water molecules inside the nanochannel is also effectively resistant to charge noises and sensitive to available charge signals.

Now we have come to the structure of aquaporins again. The structure of aquaporins is appropriate that the water molecules inside the pore are single filed. Moreover, compared to the CNT, aquaporins are much more complex while the functions of most of the structures are unknown. There are two impressive parts in those complex structures: the two highly conserved fingerprint Asp–Pro–Ala (NPA) motifs in the pore center are proposed to determine the selectivity of permeation for the channel, and the ar/R region near extracellular side, formed by the aromatic side chains of Phe and His, and Arg, is proposed to function as a proton filter [32]. We note that there are some important charged parts on these regions: the Arg residue on ar/R region is positively charged ($+1e$); the two Asn residues on NPA motifs can be considered to be carrying an effective charge of $+0.5e$ on each residue, since they are at the ends of two α-helixes (it is known that an α-helix has a net dipole moment whose magnitude corresponds to a charge of 0.5–0.7e at each end of the helix [41]). With further steps to understand the functions of those parts in the aquaporins and trying to design nanochannels inspired by aquaporins, we assign the charges on those parts near a CNT, as shown in Fig. 1.30.

Explicitly, an SWNT 23 Å in length and 8.1 Å in diameter is embedded along the vertical direction between two graphite sheets, and three positive charges with charge magnitudes of 1.0e, 0.5e, and 0.5e are positioned at $z = -d$, −0.7 Å, and 0.7 Å, respectively, where $z = 0$ corresponds to the center of the channel. All of the positive charges are at the same radial distance, δ, from the carbon atoms. Numerically, they have found that when $\delta \approx$ 0.5 Å, there is a considerable net flux from top to bottom.

1.1.2 Manipulating Biomolecules with Aqueous Liquids Confined Within Nanoscale Channels

One thing we are inspired from this molecular water pump is that there is a strong interaction between the charge outside the nanotube and the water molecules inside the nanotube. This is because of the ordered dipole orientations of the water molecules inside the nanotube when there is a charge outside the nanotube. It is the ordering of the water dipole orientations that makes the interaction between the charge and the water molecules strong. In Fig. 1.31, we have shown the averaged dipole orientation $<\theta>$ of water molecules when there is a charge outside the nanotube (see inset in Fig. 1.32), where r is the distance of a water molecule inside

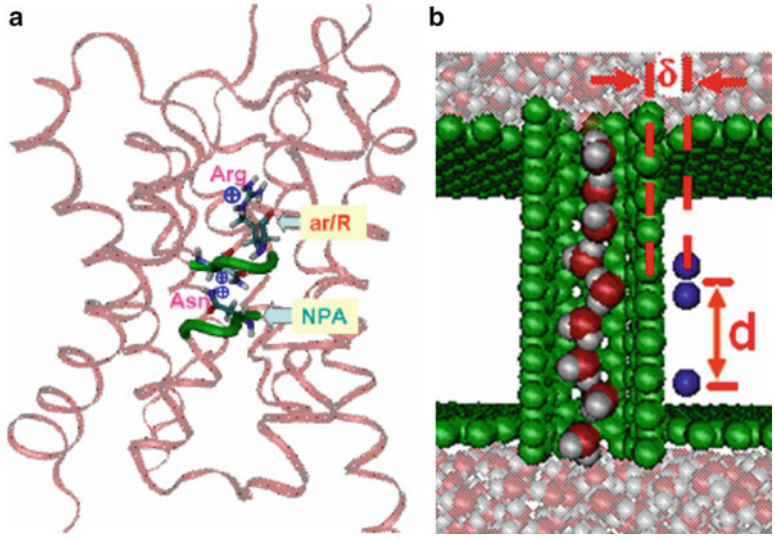

Fig. 1.30 Structure of AQP1 together with a scheme of the molecular water pump. (**a**) Ribbon diagram of the structure of AQP1. Two NPA regions are in green tube form. The ar/R region is around the Arg residue. The Arg and Asn residues are in licorice form. The Arg residue has a $+e$ net charge, and the two Asn residues on NPA motifs can be considered to carry an effective charge of $+0.5e$ on each residue (see text for details). The X-ray structure of AQP1 is obtained from Protein Data Bank (PDB) (reprinted from [18]. Copyright 2008 Institute of Physics, UK) (**b**) snapshot of the system, side view. The *green spheres* are the carbon atoms of the nanotube and the graphite sheets. The *blue points* are the positive charges. The figure is not drawn to scale that the sizes of water molecules and charges are enlarged (reprinted from [43]. Copyright 2007 Nature Publishing Group)

the nanotube and the external charge, θ, is defined as the angle between the dipole orientation of the water molecule and the line connecting the oxygen of the water molecule and the external charge. It is clear that $<\theta>$ approaches 90° when r is large enough, and the departure of $<\theta>$ from 90° shows the ordering of the water orientations. We can even predict the electrostatic interaction energy of the external charge with a water molecule at r, denoted by E_{theory}, from this $<\theta>$ distribution with the dipole moment for each water molecule ($0.489e$ Å in the TIP3P water model). As is shown in the figure (red symbols •-•), E_{theory} agrees well with the simulation result $E_{\text{simulation}}$ (the black symbols ■-■).

With this observation, we can manipulate a drop of water in the nanotube by a charge outside the nanotube. When there is a biomolecule in the water drop, we can even manipulate its position. As the charge moves along, the water–peptide mixture will follow it inside the nanotube. As the example shown in Fig. 1.32, we have shown the x-coordinate of the COM of the peptide and the peptide–water mixture as a function of time together with the x-coordinate of the external charge. We can see that the peptide–water mixture shows controllable movement by the manipulation of external charge [42]. As we know, encapsulating the molecules into

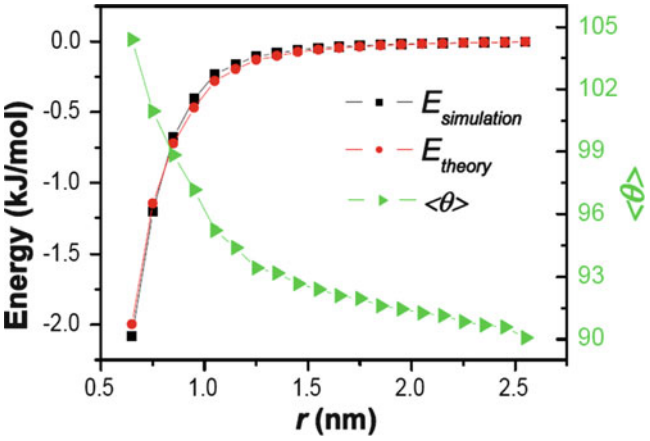

Fig. 1.31 Water–charge electrostatic interaction energy (E_{theory} *and* $E_{\text{simulation}}$) together with the averaged dipole orientation of water molecules $<\theta>$ (*green* and *right Y*-axis) with respect to the distance between a water molecule and the external charge for $q = 0.5e$. E_{theory} (*red symbols*) is computed from the $<\theta>$ distribution and $E_{\text{simulation}}$ (*black symbols*) is determined directly from numerical simulations (reprinted from [42]. Copyright 2009 American Chemical Society)

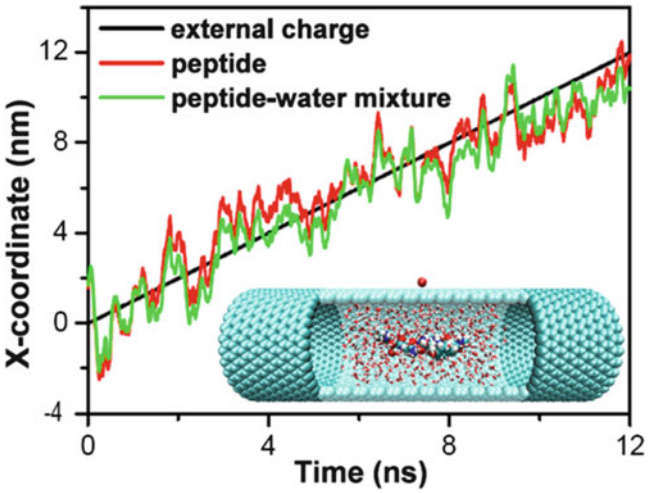

Fig. 1.32 *X*-coordinate of the center of mass of the peptide and the peptide–water mixture as a function of time, together with the *x*-coordinate of the external charge for the effective charge $q = 0.5e$. Inset: a water droplet with the peptide (GNNQQNY) in a single-walled carbon nanotube (SWNT) together with a charge (*big redsphere*) outside the tube. The *light bluespheres* represent the SWNT. Some carbon atoms of SWNT are not shown or drawn transparent for demonstration. The other colored spheres in the middle of SWNT are the atoms of the peptide

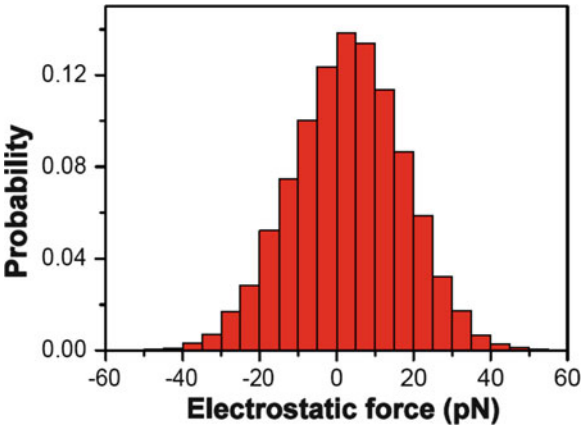

Fig. 1.33 The electrostatic forces by the external charge exerting on the peptide–water mixture along the *x*-axis for the case of System I when $q = +0.5e$. The positive direction of the force is the positive direction of the *x*-axis, and a 5 pN force interval is used (reprinted from [42]. Copyright 2009 American Chemical Society)

nanoscale pores can lead to interesting properties and behaviors that significantly differ from those of bulk systems [6, 21, 22, 32, 40, 43–59], including the enhanced catalysis [44, 45] and enhanced stability of the native structure of proteins [47], new folding mechanisms of proteins [49, 50], ordered water structure [52–54], extrafast motion of water molecules [6, 21, 46], non-Fickian-type diffusion [55], and excellent on–off gating behavior [22, 40]. Furthermore, it has been found that when the molecules are confined in nanosized water droplets [60, 61], their structures, hydrophobic and ionic interactions differ from those in bulk water [62, 63]. Manipulating the positions of the molecules encapsulated in the nanopores with respect to time is important in controlling the interactions or chemical reactions of the inner molecules. In recent years, there have been considerable efforts [14, 64–70] devoted to the study of the translocation/permeation of molecules along/through the nanochannels. Yeh and Hummer used an electric field to drive the charged macromolecules through nanopores [64]. Longhurst and Quirke made use of capillary force to draw decane molecules into an SWNT and temperature difference to drive their transport through the SWNT [67]. Zhao et al. demonstrated experimentally that a water flow can be driven by the applied current of the SWNT [14]. Král used laser to excitate an electric current in the CNT, thus resulting in a net force on ions absorbed in the nanotube [70].

We have also calculated the electrostatic force that the external charge exerts on the peptide–water mixture along the *x*-axis. The electrostatic forces dominatively range from −40 to +40 pN (see Fig. 1.33), which fall within the working ranges of many existing techniques such as STM and AFM. This result suggests that the AFM/STM tip carrying charge(s) may be able to manipulate the peptide with aqueous liquids according to the method described here.

Furthermore, on the basis of the above design, we can controllably move two biomolecule–water mixtures together conveniently for the interaction of the two biomolecules, as demonstrated in Fig. 1.34. Here, we use the same peptides used

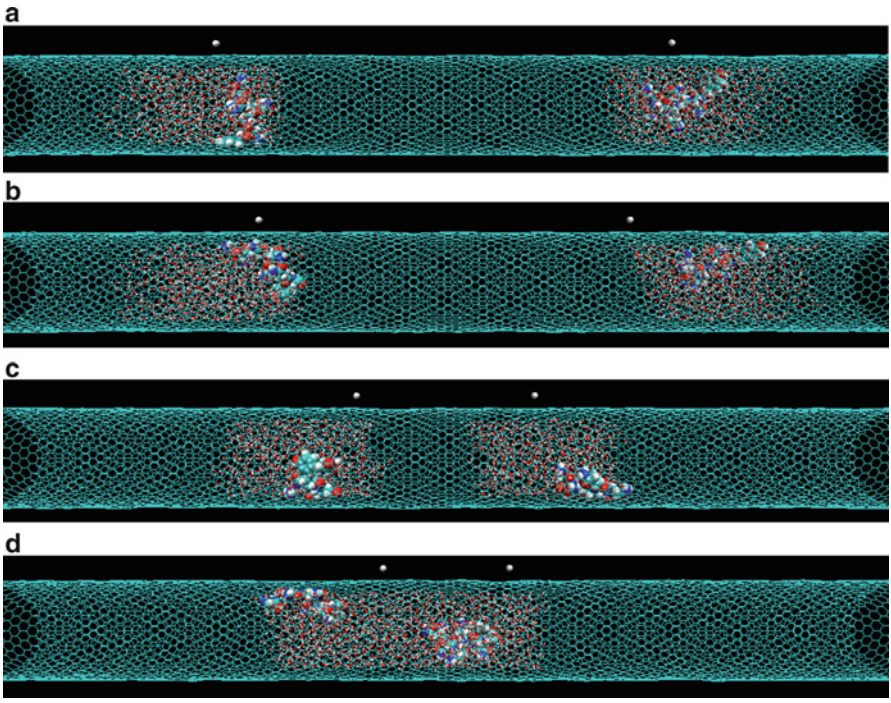

Fig. 1.34 Controllable moving of two biomolecule–water mixtures together. The *light greenlines* (linked hexagons) represent the SWNT. The colored spheres inside SWNT are the atoms of the peptide. The *white spheres* outside the SWNT are the external charges (each has a value of $+0.5e$) and the *red–white dots* are the water molecules

in the text (Ace–GNNQQNY–NMe) for demonstration. Each external charge has a value of $+0.5e$. The counterion with a value of $-1e$ is constrained at the edge of the box.

There are many factors affecting the manipulation. First, let us discuss the influence of the quantity of the external charge on the manipulation. Thermal fluctuation will sometimes make the manipulation unsuccessful, but for $q = \pm 1.0e$, this is a rare event. When $q = \pm 0.5e$, we have observed that the peptide–water mixture follows the external charge in 8 of the 11 simulations for the same systems with different initial conditions. In the cases where $q = \pm 0.33e$ and $\pm 0.25e$, the peptide–water mixture has low probabilities to follow the external charge.

Second, we have found that the speed of the external charge has a remarkable influence on the manipulation. When the speed of the external charge increases from 1 to 10 m/s, only one successful manipulation is observed in ten simulations with different initial conditions. We expect that as the speed of the external charge decreases, the probabilities for these unsuccessful cases decrease. Usually, the speed of the AFM/STM tip is within the magnitudes from 1 nm/s to 1 μm/s. Considering that the speed of the external charge in our simulation is up to 1 m/s, the rate

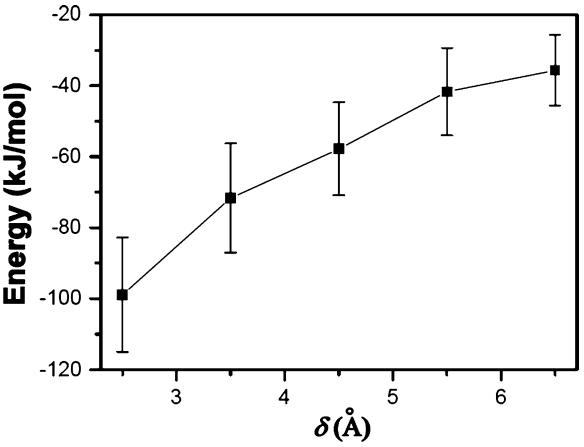

Fig. 1.35 The electrostatic interaction energies between the external charge and the water molecules with respect to the distance of the external charge from the tube wall (defined by δ) for the case of System I when $q = +1e$. The *error bars* show the fluctuations due to thermal noise (reprinted from [42]. Copyright 2009 American Chemical Society)

for a successful manipulation may even be higher for a much lower speed under experimental conditions. When the peptide is substituted by a larger molecule such as a protein, the effective value of the external charge required for successful manipulation should be larger. We note that in the case where the probability of the successful manipulations by a single charge is low, we can use a series of charges, which can greatly enhance the successful probabilities.

Third, the distance of the external charge from the tube wall (defined by δ) also influences the manipulation. For System I, as is shown in Fig. 1.35, the electrostatic interaction energy between the external charge with the effective value of $q = +1e$ and the water molecules in the peptide–water mixture increases gradually as δ increases. Numerically, our simulation shows that even when δ is up to 6.5 Å, the peptide–water mixture can also follow the external charge well. When $q = +0.5e$, we have observed two of the three cases with different initial conditions that the peptide–water mixture follows the external charge in 12 ns simulation when the distance is 5.5 Å, with an electrostatic interaction energy between the external charge and the water molecules of -10.5 ± 6.3 kJ/mol, obtained from the successful manipulation cases.

Finally, since our simulations are based on the stochastic dynamics, the damping coefficient used will influence the manipulation. For System I, when the damping coefficient $\xi = 0.01$ ps^{-1}, according to the Langevin equation, the force due to Langevin damping is $f_{\text{damping}} = M\xi v = 0.153$ pN, in which M is the mass of peptide–water mixture, if we assume that the peptide–water mixture follows the external charge extremely well with the same velocity $v = 1$ m/s. This value of f_{damping} is much smaller than the electrostatic force that the external charge exerts on the water molecules. We find that some modifications of the value of ξ do not change the results much in this chapter. Our calculation shows that when $\xi = 0.1$ ps^{-1}, the electrostatic interaction energy is -17.0 ± 8.5 kJ/mol ($q = +0.5e$), which is very close to the value of -18.5 ± 7.9 kJ/mol for $\xi = 0.01$ ps^{-1} case; moreover, the peptide–water mixture still follows the external charge well in the 12 ns simulation

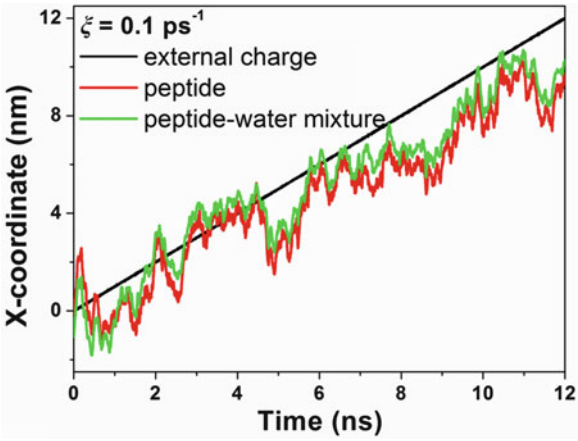

Fig. 1.36 The influence of larger damping coefficient ξ ($\xi = 0.1$ ps^{-1}) on the manipulation. *X*-coordinate of the center of mass of the GNNQQNY peptide (in *red*) and the peptide–water mixture (in *green*) vs. time, together with the *x*-coordinate of the external charge (in *black*) for the case of System I when $q = +0.5e$. As a comparison, Fig. 1.9 shows the manipulation when $\xi = 0.01$ ps^{-1}

time (see Fig. 1.36). We note that, in this case, the peptide or peptide–water mixture gets behind the external charge in most of time due to the larger Langevin damping force; in contrast, in the case of $\xi = 0.01$ ps^{-1}, the peptide or peptide–water mixture usually goes ahead of the external charge due to thermal fluctuation. Moreover, we have also carried conventional MD simulation: the controllable manipulation abilities are consistent with the results presented here.

The aforementioned design can be regarded as an "indirect" approach, which manipulates the position of biomolecule through manipulating the position of water molecules surrounding it. We also propose a "direct" approach, which can manipulate the position of biomolecule with charged residue(s) inside a water-filled nanotube directly. To demonstrate this design, we have built another system, namely, System II. It contains a peptide called Aβ_{16-22} [71] (Ace–KLVFFAE–NMe) inside a (29, 0) zigzag SWNT with dimensions of 8.33 nm in length and 2.24 nm in diameter (see Fig. 1.37). This peptide is an Alzheimer's disease-related peptide, having a lysine (K) residue with one positive charge ($+1e$) at one end and a glutamic acid (E) residue with one negative charge ($-1e$) at the other. The other space in SWNT is fully filled with water. The SWNT is aligned along the *x*-axis in a periodic box of $8.4 \times 12 \times 12$ nm^3. A group of external charges that contained 12 charges forming a 3×4 array is allocated 3.5 Å from the SWNT wall and initially above the glutamic acid residue of the peptide. The distance between the nearest adjacent charges is 2.88 Å. This charge pattern is very similar to the Au (100) crystal face. We note that other patterns of the external charge group do not change much the conclusion we have obtained here provided that the external charges are densely packed in two dimensions. The quantity of each charge is also denoted by q. The corresponding counterions are constrained at the right edge of the box to make the system neutral.

For the case of System II, Fig. 1.38 shows a typical example of the *x*-coordinate of the COM of the peptide as a function of time, together with the *x*-coordinate of the geometrical center of the external charges for $q = +0.5e$ per atom. The peptide

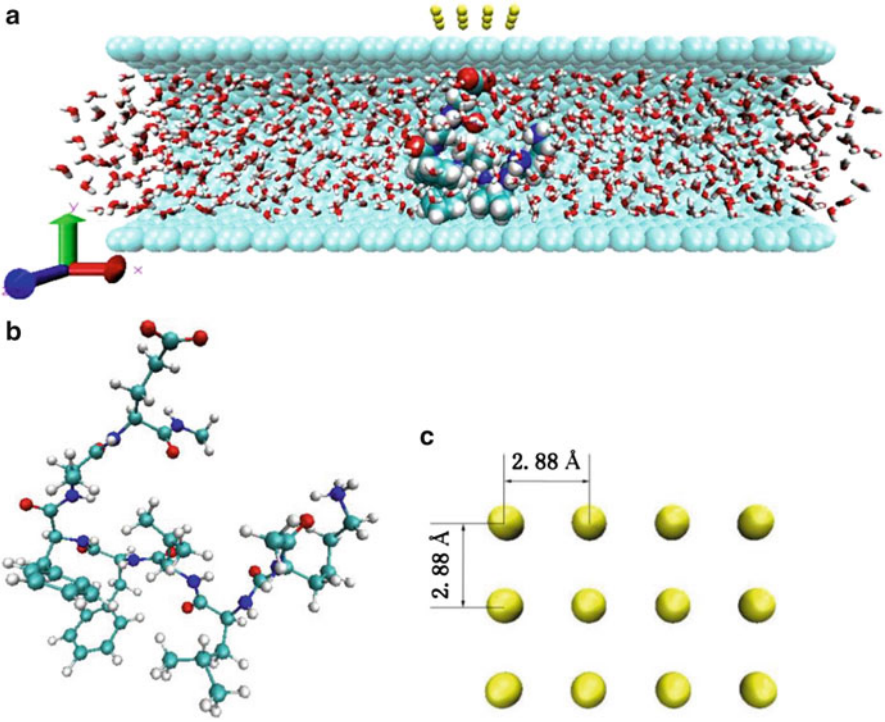

Fig. 1.37 The simulated system (System II). (**a**) Initial framework of System II. The SWNT (*light bluespheres*) is fully filled with water molecules (*red-white pillars*). Some carbon atoms of SWNT are omitted for clarity. The other colored spheres in the middle of SWNT are the atoms of the $A\beta_{16–22}$ peptide. The *yellow spheres* outside the nanotube stand for the external charges (reprinted from [42]. Copyright 2009 American Chemical Society) (**b**) initial structure of $A\beta_{16–22}$ peptide (Ace–KLVFFAE–NMe). It contains a lysine (K) residue with one positive charge ($+1e$) at one end and a glutamic acid (E) residue with one negative charge ($-1e$) at the other. (**c**) Structure of the lattice of external charges, which contains 12 charges forming a 3×4 array. The distance between the nearest adjacent charges is 2.88 Å

follows the external charges very well. In the six simulations we have performed with different initial conditions, only in one simulation the peptide does not follow the external charges.

We have computed the electrostatic interaction energy of the external charges with the peptide vs. time, shown in Fig. 1.39. The average electrostatic interaction energy (averaged over five successful manipulation cases) is -704 ± 142 kJ/mol. In all simulations, the distances between the COM of the peptide and the geometrical center of the external charges range from 1.2 to 2.6 nm with an average value of 1.6 nm. We have noted that the deprotonated carboxyl group (COO) on the glutamic acid residue of the peptide carries most ($-0.9e$) of the negative charge of the whole residue ($-1e$). Since the external charges are positive, the interaction between the peptide and the external charges is dominated by the interaction between the

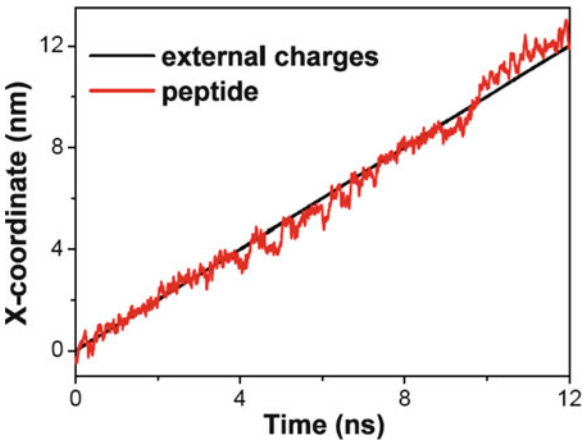

Fig. 1.38 Manipulating the peptide with charged residues inside a water-filled nanotube (i.e., System II). The x-coordinate of the center of mass of the Aβ_{16-22} peptide (*red line*) as a function of time, together with the x-coordinate of the geometrical center of the external charges (*black line*) (reprinted from [42]. Copyright 2009 American Chemical Society)

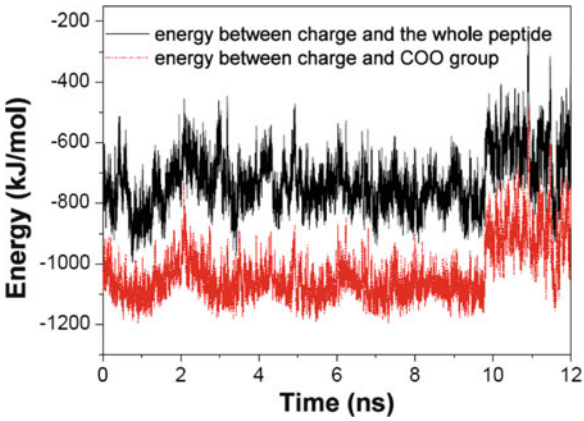

Fig. 1.39 Electrostatic interaction energy of the external charges with the Aβ_{16-22} peptide and with the deprotonated carboxyl group (COO) as a function of simulation time

COO group and the external charges. Numerically, we have found that the average electrostatic interaction energy of the external charges with the COO group is -973 ± 143 kJ/mol, quite close to the electrostatic interaction energy of the external charges with the peptide (see also Fig. 1.39). Likewise, the distances between the COM of the COO group and the geometrical center of the external charge range from 0.6 to 2.2 nm with an average value of 0.8 nm. These distances are smaller than the distances between the COM of the peptide and the geometrical center of the external charges. Consequently, the manipulation of the peptide mainly results from the tight trapping of the COO group by the external charges.

We have also calculated the electrostatic forces that the peptide and water inside the nanochannel exert on the external charges along the x-axis. The forces range from -600 to $+600$ pN (see Fig. 1.40), which also fall within the working ranges of many existing techniques such as STM and AFM.

The number of the charges in the externally charged group is important for the manipulation. We have found only one successful case in five simulations with

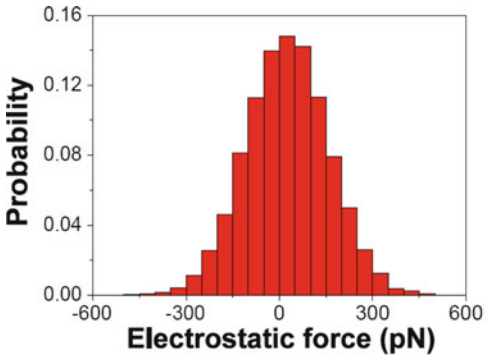

Fig. 1.40 The electrostatic forces that the peptide and water inside the nanochannel exert on the external charges along the *x*-axis for the case of System II. The positive direction of the force is the positive direction of the *x*-axis, and a 50 pN force interval is used

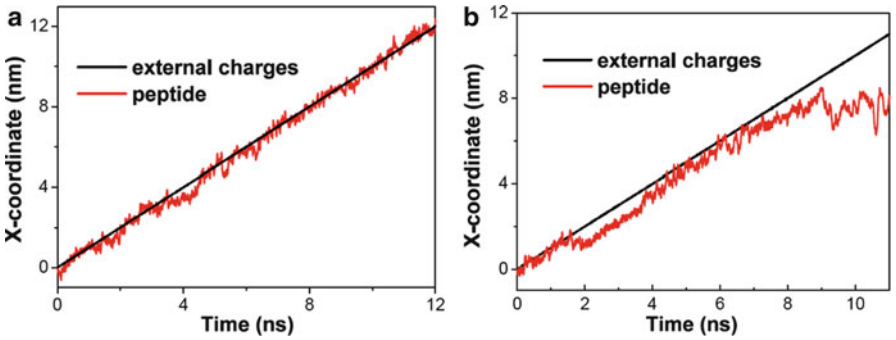

Fig. 1.41 Manipulating the peptide with charged residues inside a water-filled nanotube when the number of external charges reduces to nine (in a 3×3 array with $q = 0.5e$ per atom). *Red* and *black lines* represent the *x*-coordinate of the center of mass of the $A\beta_{16–22}$ peptide and the geometrical center of the external charges, respectively, as a function of time. Only one successful case is observed (**a**) in five simulations. (**b**) A typical unsuccessful manipulating case

different initial conditions when there are only nine charges in a 3×3 array with $q = 0.5e$ per atom (see Fig. 1.41). When the group of external charges is substituted by one externally charged atom, the minimal value of the external charge required for manipulation is around $+3e$. It seems that the manipulation of the peptide inside a water-filled SWNT is much more difficult than the manipulation of the peptide in a drop of peptide–water mixture inside an empty SWNT.

The peptide used here has only one negatively and one positively charged residue and is neutral as a whole. It should be noted that many biomolecules with highly charged fragments may not be neutral. For example, the peptide LDTGADDTVLE [72], which is the fragment 24–34 of the protease of the human immunodeficiency virus type 1, has a total of $-4e$ charges because of the presence of three aspartic acid (D) residues and one glutamic acid (E) residue, all of which are negatively charged, and the absence of positively charged residue. It could be expected that for this kind of biomolecules, the manipulation becomes more effective.

Finally, we note that we have not considered the possible metal semiconductor property of the nanotube. For those nanotubes, the screening effect should be considered, and the charges used here should be regarded as effective charges. It is interesting to note that even for the metallic nanotube, the interaction between a charge outside the single-walled nanotube and the charges inside the nanotube is still quite strong. However, insulator nanochannels may be much better in the application, which is expected to be fabricated in the future. Considering that the external charges required for these manipulations are quite small, which are still available after taking into account the screen effect of many nanotubes, our designs may serve as lab-in-nanotube for the interactions and chemical reactions of molecules especially biomolecules and hence may have wide applications in nanotechnology and biotechnology.

1.1.3 Signal Transmission, Conversion, and Multiplication with Polar Molecules Confined in Nanochannels

Another thing we are inspired from the one-dimensional hydrogen bonds chain as shown in Fig. 1.2 is that the highly stable chain can be used in the signal transmission, conversion, and multiplication at nanoscale and/or molecular scale. Nanoscale structures or molecules have been utilized as the elements in electronic devices [73–76], such as nanowires, switches, rectifiers, and logic circuits, and the integration of these molecular-based devices and other nanoscale structures has led to a number of demonstrations of new and useful applications [77, 78]. Particularly, electrical transportation [79], electrical and partity switching [73–76], and chemical and biomolecular sensors [80, 81] have been developed based on nanowires or nanotubes. Biosensors for DNA diagnostics, gene analysis, fast detection of warfare agents, and forensic applications have also been achieved by electrochemical method[14] and microarrays[17] together with the particular behavior of biomolecules in nanoscale [82].

In biology, signal representations are often related to electrical changes. For example, in central nerve systems, the most common mechanism for signaling between neurons is the neurotransmitter-releasing chemical synapse, but faster and simpler signaling can be achieved with electrical synapses, specialized junctions (gap junctions) that mediate electrical coupling between neurons [83–86]. Electrical coupling mediated by electrical synapses is an important feature of local inhibitory circuits and plays a fundamental role in the detection and promotion of synchronous activity (firing pattern) within the neocortex [87–89]. In fact, weak coupling may lead to antiphasic or asynchronous firing [83, 84, 90].

On the other hand, although it has been of great interest to study the mechanism of signal transmission, conversion, and multiplication at molecular level, molecular details in these systems remain largely unknown due to the intrinsic complexity in these molecular systems and the significant noises arising from thermal fluctuations

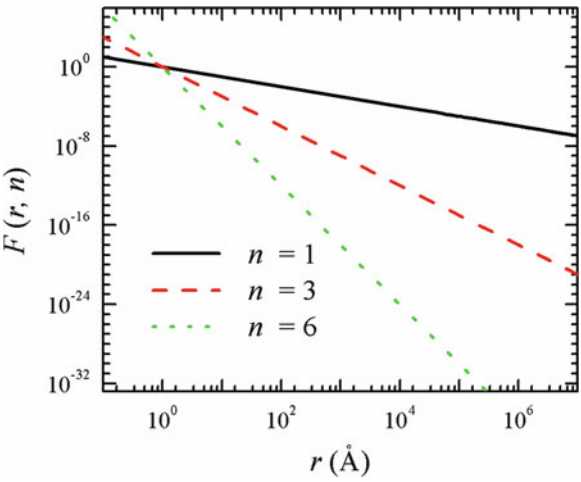

Fig. 1.42 Curves for function $F(r, n) = A_n\ (r/r_0)^{-n}$ for $r_0 = 1$ Å and $n = 1, 3, 6$, and $A_n = 1$ (reprinted from [132]. Copyright 2010 Royal Society of Chemistry)

as well as interferences between branch signals. For example, we note that the signal transmission along intercellular and intracellular pathways and between the exterior and the interior of a cell may be mediated by protein allostery [91–93], which may lead to the redistribution of the charges and the reorientations of the charge dipoles in the proteins, but the exact molecular mechanism is still unclear.

As we have known, thermal noises usually hold important interference in signal transmission, conversion, and multiplication. Particularly at the nanoscale, thermal noises often significantly reduce the signal strength during the transmission, conversion, and multiplication.

More critically, it should be noted that the interferences between signals can be very strong if the signals are transmitted by charges. In terms of Coulomb's law, the interaction potential between two charges decreases with respect to r^{-1}, where r is the distance between those two charges. At the nanoscale, this slow decay will result in strong interaction between two charges (signals). Therefore, within one nanometer's distance, although the VDW interaction almost decreases to zero with respect to r^{-6}, extremely faster than r^{-1}, the interaction cannot be neglected between two atoms yet. As a comparison in Fig. 1.42, we show a diagram of the function $F(r, n) = A_n\ (r/r_0)^{-n}$ with respect to r for $r_0 = 1$ Å and $n = 1, 3, 6$, where A_n is set as a constant 1. Therein, the dipole–dipole interaction potential just has a form of r^{-3}, decaying much faster than the charge–charge interaction (r^{-1}) with distance.

It is much worthwhile making an attempt to use the dipole to transmit a signal, due to the much faster decay of the interaction between different dipole signals. Several decades ago, one began to study the properties of electric dipoles and the applications on them. The most notable one is the Ising model [94, 95]. Recently, the behavior of one-dimensional dipole chains has been discussed, including the energy transfer in a dipole chain [96], the design of a logical AND port using dipole chains with a junction [97], and the initiation of the orientation of one-dimensional dipole chains by a local field [98].

Here, we find water, as the most important matter in the world, can be designed to become an excellent medium for the transmission of signals. Water molecules confined within nanoscale channels exhibit structures and dynamics that are very different from bulk [6, 15, 17, 22, 32, 34, 43, 52, 99–103]. Particularly, in nanochannels with suitable radii, water molecules are confined to form one-dimensional chains linked by hydrogen bonding with the "concerted" water dipole orientations [21, 22, 43, 104], which provide an excellent example for the transmission of signals due to water dipole interactions. Note that the stable water molecular chain is a prerequisite for signal transmission as a medium.

Fortunately, the reorientation of this water dipole chain has its characteristic time estimated to be in the range of 2–3 ns for CNTs with a length of 1.34 nm [21]. More remarkably, the water molecule chains in a nanotube can remain dipole-ordered up to macroscopic lengths of 0.1 mm, with durations up to 0.1 s [104].

As an example, Fig. 1.43 shows the "concerted" orientations of water molecules (water dipoles are ordered cooperatively inside the CNT) [21, 22, 40, 43, 59, 104]. If we can "tune" the orientation of one water molecule using a single charge at one end, we might be able to control the orientations of other water molecules in the same channel or other connected channels. In other words, we have a molecular level "signal transmission," i.e., converting a charge signal to water dipole orientation signal (at one end) and then transmitting the water dipole orientation signal to other ends, which might be converted back to a charge signal again. Furthermore, if we use Y-shaped nanochannels, i.e., three nanochannels connected with each other to form a Y-junction, we can even achieve a "signal multiplication," which means that a water dipole orientation signal can be multiplied into many water dipole orientation signals [59]. It is also observed that the signal transmission and multiplication, via water molecules confined in nanoscale channels, can be effectively shielded from thermal fluctuations.

We have applied MD simulations, which are widely used in nanoscale- and molecular-scale simulations for both physical and biological systems [22, 59, 105–111], to investigate this interesting phenomenon of water-mediated signal transmission. NVT ensemble simulations have been carried out at a constant temperature of 300 K using a Berendsen thermostat [105] and in constant volumes ($L_x \times L_y \times L_z = 6.01\,\text{nm} \times 6.01\,\text{nm} \times 11.00\,\text{nm}$ in SWNT systems with 12,922 water molecules using the molecular modeling package Gromacs 4.0.5 [106, 108], and more settings are referred to Ref. [59]). A typical (6, 6) uncapped armchair SWNT with a width of 0.81 nm and a length of 5.13 nm is adopted as shown in Fig. 1.43. This device is constrained at the center of the simulation boxes by using the position restraints (the whole tube length is partitioned evenly into three segments with an interval 1.71 nm, and thus the four rings of carbon atoms are constrained) solvated with water molecules with constant density. We have adopted the particle-mesh Ewald method [112] to model long-range electrostatic interactions, and we have applied periodic boundary conditions in all directions. A time step of 2 fs is used, and data are collected every 0.5 ps. In all of our simulation results, the TIP3P water model is applied and the carbon atoms are modeled as uncharged Lennard-Jones particles with a cross section of $\sigma_{CC} = 0.34\text{nm}$ and $\sigma_{CO} = 0.3275\,\text{nm}$, and a

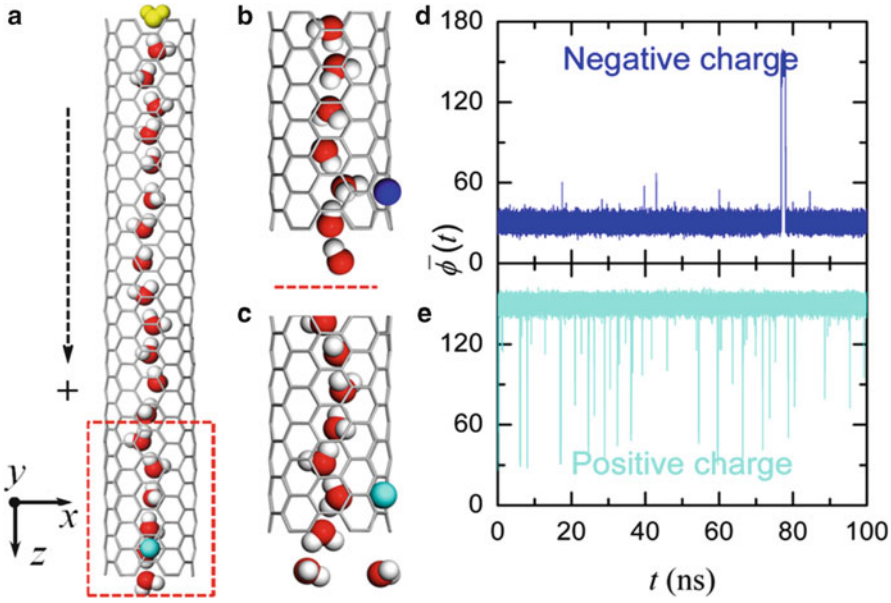

Fig. 1.43 Schematic snapshots (a, b, c) of the system with a single channel in side view (the *xz*-plane) together with the trajectories (**d**, **e**) of average dipole angle $\bar{\phi}(t)$ of the water orientations. The snapshots shown in (**b**, **c**) correspond to the *red dashed* part of the system (see subfigure a) in another side view (*yz*-plane). *Blue* and *green spheres* denote the negative charge and the positive charge, respectively, which result in different orientations of the water molecules facing the charges. The water molecule facing the external charge is named as "monitored-water." The single-walled CNT is represented by *gray lines* and its positive direction is shown by the *black dashedarrowhead*. Water molecules are shown with oxygen in *red* and hydrogen in *gray*, and the first water molecule outside the channels opposite to the charge signal input is shown in *yellow*. The dipole direction of the water molecules is not shown, which is along the midline between the two O–H chemical bonds of the water molecule. Water molecules outside the nanotubes are omitted in the figure (reprinted from [132]. Copyright 2010 Royal Society of Chemistry)

potential well depth of $\varepsilon_{CC} = 0.3612\,\mathrm{kJ \cdot mol^{-1}}$ and $\varepsilon_{CO} = 0.4802\,\mathrm{kJ \cdot mol^{-1}}$ [21]. The system is first minimized with conjugate gradient method for 10,000 steps and then equilibrated with MD for 5 ns at 300 K before data collection. An external signal charge of magnitude $1.0e$ is then introduced to the center of the second carbon ring of the main tubes (constrained by using the position restraints during the simulations), and its opposite charge for neutralization is constrained near the edge of each box at coordinates (0.00, 3.00, and 0.00 nm), which is far enough to have any meaningful influence on the signal charge (our numerical data also confirm this).

Note that at the center of a second carbon ring of the nanotube, this charge is attached in order to control the direction of the dipole orientation of the water molecule to face the charge, and we call this confined water as "monitored-water" hereafter. We have found that different signs of the charge q result in different

orientations of the monitored-water (see Fig. 1.43). Moreover, we have found that the monitored-water determined all the water orientations in the nanotube, upward or downward in concert [59]. Quantitatively, we define the water dipole orientation in the nanotube as an angle ϕ_i between the ith water molecule and the nanotube axis [59]:

$$\phi_i = \text{acos}(\vec{p}_i \cdot \hat{u}/|\vec{p}_i|),$$

where $\vec{p}_i$ is the dipole of ith water molecule and $\hat{u}$ is the axis unit vector of the nanotube. The averaged dipole angle $\bar{\phi}(t)$ is computed by

$$\bar{\phi}(t) = \sum_{i}^{N} \phi_i(t)/N(t),$$

where the average runs over all the water molecules inside a nanotube at time t, and $N(t)$ is the number of water molecules within this tube. The averaged dipole angle is used to characterize the water-mediated signal transmission. The results are shown in Fig. 1.43. It is clear that $\bar{\varphi}$ falls into very different ranges most of the time for a positive or negative signal charge: $110° < \bar{\varphi} < 170°$ for $q = +e$ and $10° < \bar{\varphi} < 70°$ for $q = -e$, indicating that the water molecules within each nanotube are well ordered (i.e., in concert). Thus, the charge ($+e$/$-e$) signal at one end of the nanotube can be readily distinguished from the dipole orientation (upward/downward) of the water molecules at the other end of the nanotube.

Next, from the aforementioned systems, the water orientation states are extracted every 10 ns after the first 30 ns of simulation time. In these states, we switch the attached charge polarity and adopt them as initial states for new next simulations. Based on these simulations with switched charge polarity, we discuss the time delay of the water orientations in response to a switch in the charge signal. Figure 1.44 display the averaged angle $\bar{\phi}(t)$ for four such scenarios. The time delay associated with the branch tubes is 3.2 ns on average, with a minimal duration of 0.04 ns (Fig. 1.44 (the last one)) and the maximal one 9.2 ns to respond to the $+e \rightarrow -e$ signal switch (which is slower) and approximately 0.07 ns only to respond to the $-e \rightarrow +e$ switch (which is much faster). This obvious disparity in the response time results from the interaction of the monitored-water with the signal charge. The negative charge attracts the two hydrogen atoms of the monitored-water and limits the mobility of the oxygen atom to a certain extent. Positive charge attracts the oxygen atom, and the two hydrogen atoms have more freedom to rotate or swing, which enables an easier switch for the configurations. This point can also be easily seen from Fig. 1.43, as we observe more fluctuations in the case with a positive signal charge. We note that the short (average 0.07–3.2 ns) response time delay implies that the signal with frequency in gigahertz range can be expected.

In response to a switch in the charge signal, it takes only tens of picoseconds for the orientation of the entire water chain to flip over inside the nanochannels. This delay time mainly results from the reorientation time of the monitored-water

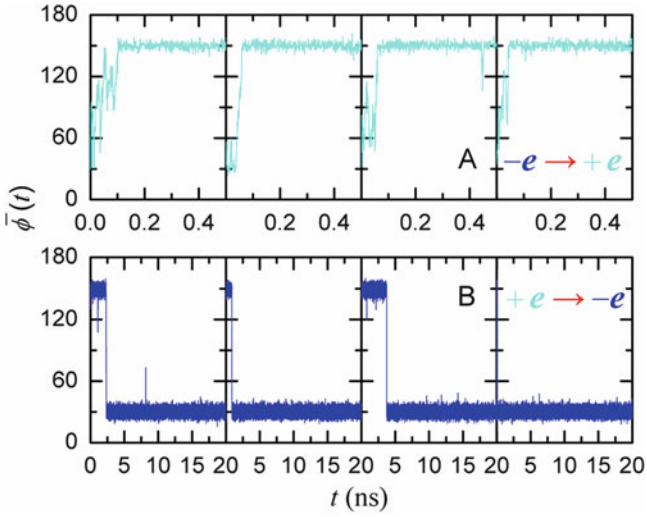

Fig. 1.44 Signal switching in an SWNT. Trajectories of the average dipole angle $\bar{\phi}(t)$ of the water orientations in an SWNT for the charge signal switch from negative to positive (*top*) and from positive to negative (*bottom*) for four typical cases with different initial states. The dipole orientations in the SWNT fully respond in approximately 0.07 ns when the charge switches from negative to positive and in 3.2 ns in the case of positive-to-negative transition (reprinted from [132]. Copyright 2010 Royal Society of Chemistry)

and its neighboring water molecules. As is shown in Fig. 1.45, a typical process displays the reorientation of water molecules in the nanochannel in response to a $+e \rightarrow -e$ signal switch. In this process, the dipoles of water chain molecules always flip over one by one, from the bottom to the top (see Fig. 1.43). In order to observe the motion of this flipping forefront point, we can trace the position of the water molecule (along the nanochannel axial direction), whose dipole angle ϕ falls into the ranges of [70°, 110°], while its two nearest neighbor molecules have their dipole angles falling into [110°, 70°] and [10°, 70°], respectively. If there is no such water molecule at any given moment, we take the position of the last-turning molecule as the current forefront. We have also plotted the value of $\bar{\varphi}$ as a function of the time. Clearly, the turning forefront is consistent with the value of $\bar{\varphi}$.

As we have seen above, charge polarity signal can transmit via the one-dimensional water dipole chain confined within nanochannels with suitable radii. More importantly, we have achieved signal multiplication at the nanoscale, making use of the Y-shaped water chain confined in the Y-shaped nanochannels.

Recently, Y-shaped nanotubes have been successfully fabricated by several different methods, including alumina templates [113], chemical vapor deposition of products generated from a pyrolysis of metallocenes [114–116], nano-welding of overlapping isolated nanotubes using high-intensity electron beams [117], and spontaneous growth of nanotube mats using Ti-doped Fe catalysts [118]. In Ref. [42], we have constructed a computational model of Y-shaped CNT, called Y-SWNT,

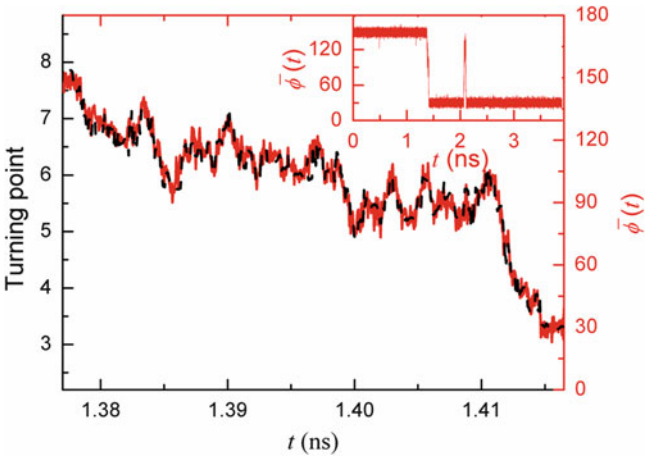

Fig. 1.45 A typical reorientation process of water molecules in nanochannel in response to a $+e \rightarrow -e$ signal switch (one data point every 50 fs). In this figure, the *red solidline* represents the detailed trajectory of the average dipole angle $\bar{\varphi}(t)$ adopting the *left* and *bottom axes* (inset shows its whole trajectory in a longer period). This trajectory indicates that the reorientation of the whole water chain is carried out by turning over the orientations of the water molecules one by one. The *black dashedline* shows this turning position in nanochannel as a time function using the *top* and *right axes* (reprinted from [132]. Copyright 2010 Royal Society of Chemistry)

as shown in Fig. 1.46. Explicitly, the Y-SWNT is obtained by joining three SWNTs symmetrically, with an angle of 120° among them. Interestingly, we have found that the behavior of the water orientations inside one branch channel can be controlled by the water orientations in another branch channel. In the following, for easy discussion, we name the three branch tubes as the main, first branch, and second branch tubes, which are denoted by MT, BT_1, and BT_2, respectively, as shown in the figure.

We still perform the MD simulations in NVT ensemble, with similar simulations methods and parameters above (all settings are referred to Ref. [59]). The Y-SWNT device is constrained by using the position restraints at the center of the simulation boxes, solvated with water molecules with constant density. An external signal charge of magnitude $1.0e$ is then introduced to the center of the second carbon ring of the main tubes (constrained by using the position restraints during the simulations), and its opposite charge for neutralization is constrained near the edge of each box at coordinates (0.00, 3.00, and 0.00 nm), which is far enough to have any meaningful influence on the signal charge (our numerical data also confirm this). These charges are introduced to the system after initial equilibration in order to observe the response time of water dipole reorientation upon the charge signal.

Obviously, a Y-shaped water chain is formed in Y-shaped nanochannels, and the water chains in different nanotubes interact with one another at the Y-junction. This usually affects the water dipole orientations in different tubes. Surprisingly, water dipoles are still in concert, just like those in the single channels. We have

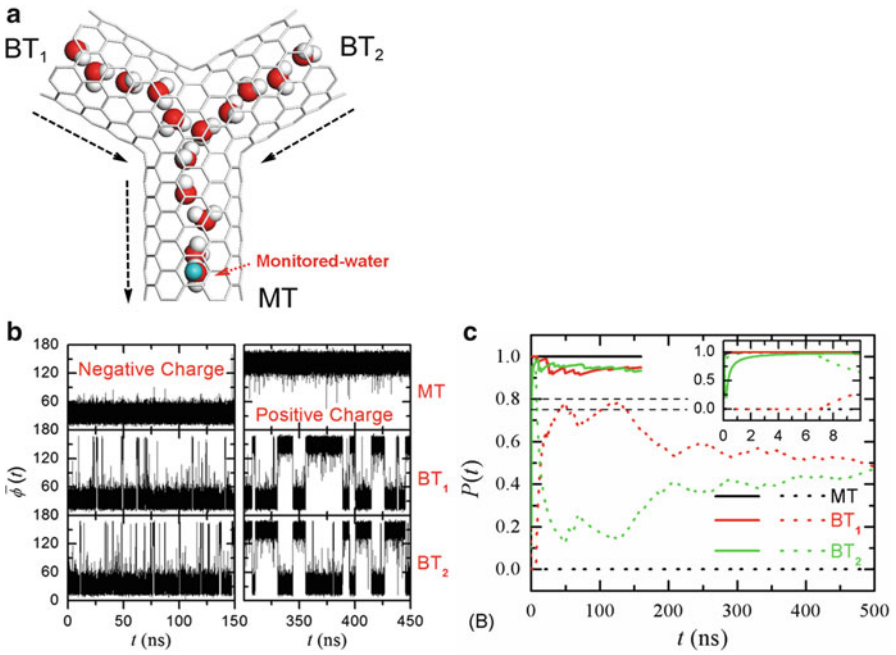

Fig. 1.46 (**a**) A schematic snapshot of the simulation system in side view (the *xz*-plane). The Y-SWNT features a main tube (MT) and two branch tubes (BT_1, BT_2) positioned in the same plane (the *xz*-plane). The angle between each two neighboring SWNTs is 120°. Small angular changes do not affect the results. The single-walled CNTs are represented by *gray lines*. Water molecules are shown with oxygen in *red* and hydrogen in *gray*. Water molecules outside the nanotubes are omitted in the figure. The *green sphere* represents the imposed charge. The lengths of MT, BT_1, and BT_2 are 1.44, 1.21, and 1.21 nm, respectively. (**b**) The average dipole angle $\bar{\varphi}(t)$ of the water orientations inside the MT, BT_1, and BT_2 for a negative charge (*left*) and a positive charge (*right*). (**c**) The probabilities of the dipole orientations $P(t)$ in different tubes for a negative charge (*solid lines*) and a positive charge (*dashed lines*). $P(t)$ for a negative charge converges to about 1.0 within a few nanoseconds (reprinted from [59]. Copyright 2009 National Academy of Science, USA)

adopted the similar approach that an external charge q is attached at the center of a second carbon ring of the MT (see Fig. 1.46) to initiate a signal of water dipole orientations. Similar to the single channels, the water molecules in the MT have the upward and downward concerted dipole orientation for $q = -e$ and $q = +e$, respectively. Remarkably, the water orientations in both the BTs follow the water orientations in the MT when water orientations in the MT are downward, while the water orientations in both the BTs fluctuate between upward and downward when the water orientations in the MT are upward. This can be seen more clearly from the time-dependent behavior of $\bar{\varphi}(t)$ as shown in Fig. 1.46. Therefore, from the water orientations in each branch tube of the Y-shaped channel, we can easily distinguish the sign of the imposed charge at the MT. In other words, the charge signal at the bottom of the MT is "converted" into water dipole signal and then transmitted to the two Y-branch tops and "multiplied" (from one signal to two).

We characterize the water-mediated signal multiplication, by computing the probability of occurrence in the range of $10° < \bar{\varphi} < 70°$, denoted by $P(t)$. We can expect that $P(t)$ approaches 1 in both BTs when the water orientations in the MT are downward (after a sufficiently long time). In contrast, $P(t)$ approaches 0.5 in both BTs when the water orientations in the MT are upward, since the water orientations in both BTs fluctuate between upward and downward with a roughly equal probability. If we set P_C as a value between 0.5 and 1, we expect that $P > P_C$ in the BTs corresponds to the downward water orientations in the MT and that $P < P_C$ in the BTs implies the upward water orientations in the MT after a sufficiently long time. Considering the rapid convergence of the case for the downward water orientations in the MT, $P_C = 0.8$ is set, which is a little larger than the average value of 0.5 and 1. From Fig. 1.46, we can see that $P > P_C$ in both BTs for any time $t > 1$ ns for the downward water orientations in the MT, while $P < P_C$ in both BTs for any time $t > 8$ ns for the upward water orientations in the MT. Thus, the charge signal at the MT can be readily distinguished from the value of $P(t)$ in each BT within a time interval of 8 ns with an appropriate threshold $P_C = 0.8$.

In the following, we further examine the water orientations inside the branched tubes (BTs). Let us first consider a single channel without any external charge. There is a hydrogen atom pointing out at the upmost (or bottommost) end when water molecules inside the channel have a concerted upward (or downward) orientation inside the single channel. One upward → downward switch of the water orientations inside the nanochannel will result in an "apparent" transportation of an upward-pointing hydrogen atom at the upmost-end of the tube to a downward-pointing hydrogen atom at its bottommost-end.

However, there is a different situation in Y-shaped nanochannels. Let us think about what happens to the water orientations inside a Y-shaped nanochannel. In the MT, there is the similar bottom → upper transportation of only one hydrogen atom, after the downward → upward switch of its concerted water orientation. But this transportation causes a different situation in the BTs. There is the transportation of only half a hydrogen atom on the average in each BT, due to the conservation of the hydrogen atom (the total number of the hydrogen transportation is also one for both BTs). Different from the above simple single-tube case, this creates asymmetry for the Y-shaped tube, since the average half hydrogen atom "transported" in BTs can be either zero or one at any moment. Thus, the situation will not be always a simple upward → downward (or downward → upward) orientation switch in each BT following that in the MT. In other words, if the water orientations in both BTs follow the *downward* water orientations as in the MT, these same water orientations in both BTs might not follow the *upward* water orientations as in the MT on the other hand.

Interestingly, our simulations exactly reproduce this situation. For example, the downward water orientations in both BTs are observed when the water orientations in the MT are downward (corresponding to a negative monitored charge), while the upward water orientation in the MT (corresponding to a positive monitored charge) results in a fluctuation of the water orientations between the downward and upward

orientations with a roughly equal probability in the BTs. This behavior can be partly explained from the interactions of water molecules at the Y-junction. When the water orientations are downward in the MT, the O atom of the uppermost water molecule in the MT attracts two H atoms from the two bottommost water molecules in the BTs; on the other hand, when the water orientations are upward in the MT, one of the H atoms of the uppermost water molecule in the MT attracts both O atoms in the bottommost water molecules in the BTs. The interaction in the former case is much stronger than interaction in the latter case. Consequently, the average value of $P(t)$ in the branch tubes is 0.5 for a concerted upward water orientation in the MT (corresponding to a positive monitored charge).

In Y-shaped nanochannels, water reorientation also holds its time delay in response to a switch in the charge signal [59]. In our simulations, the time delay associated with the BTs is found to be slow, 40 ns on average with a maximal duration of 150 ns, to respond to the downward → upward signal switch of the water orientations in the MT, but much faster, 4 ns only, to respond to the upward → downward switch of the water orientations in the MT. Clearly, the former has longer delay time than the latter. This is because that the downward water orientations in the MT (where one O atom controls two H atoms at the Y-junction) are much more stable than the case for the upward water orientations in the MT (where one H atom controls two O atoms at the Y-junction). It takes more time to shift from a more stable state to a less stable one. Compared to the time delay for switches in a single nanochannel (0.07–3.2 ns), the response times in the Y-channels are also generally longer, particularly for the downward → upward switch.

We emphasize that the stability of water chain confined in nanochannels is a guarantee to achieve water-mediated signal transmission, conversion, and multiplication. The phenomenon that we have observed is robust. First, we note that the signal multiplication capability is not very sensitive to the angles of the Y-shaped tube (the angles between SWNTs, currently at 120°, 120°, 120°). We have tried T-shaped tubes (with an angle of 90°, 90°, 180°) and other slightly different angles, and the results are more or less the same in terms of water orientation propagations.

Next, the orientation of the monitored-water and, consequently, the orientations of the all water molecules in the nanotubes can be controlled by a single charge with a quantity of one electron. This is a remarkable capability from the viewpoint of the signal transmission and conversion. Thus, what is the minimal charge needed for this capability? Numerical analysis shows that the magnitude of this signal charge needs to be larger than $0.6e$—our data using a charge from $0.6e$ to $1.0e$ indicate that the water orientations can be well controlled with such a single charge. From the previous discussion [22], it is clear that the orientation of the monitored-water can be "fixated" only when the electrostatic interaction energy between the external charge and the monitored-water is comparable to the interaction energy of the monitored-water with either side of its neighboring water molecules. Since the imposed charge is placed at the center of a second carbon ring of the nanotube, which has a distance of about 4 Å from the centerline of the nanotube (close to the distance between two water neighboring molecules), the charge required to control the orientation of the

monitored-water should probably be larger than the partial charge on each hydrogen atom (e.g., 0.417e in TIP3P water model). This is consistent with our numerical observation.

On the other hand, for the practical applications, it is very important to output the water dipole signal. As we have shown above, there is a hydrogen (oxygen) atom with a partial positive (negative) charge at the end of the nanochannel when the water dipole chain is pointing outward (inward). This partial charge can trigger (or control) a neighboring polar molecule or charge outside the channel (e.g., see Fig. 1.43, for the yellow-colored first water molecule outside the channel). Since all the water molecules share the same dipole orientation as the first water molecule inside the nanochannels, the overall water dipole moment might be large enough to be detected. This dipole moment has a value of several Debyes [59] and can interact with the electric field. We note that the semiconductor or conductor properties of some nanotubes may screen the dipole moment interacting with electric field. Insulator nanochannels, which may be fabricated in the future, might be better for this application.

Finally, via dipole–dipole interaction, with relevant interference at nanoscale, we can achieve signal transmission, conversion, and multiplication. As an important view, since water is not the only polar molecule with a dipole moment, we expect that other polar molecules, such as urea or ethanol, might have the same capability to transmit and multiply signals inside nanotubes. These small molecules, especially water, have some unusual and important physical and chemical properties, including their interactions with proteins [99,100,107,119]. In fact, as a fundamental property of all cells, cell polarity has already played a central role in signal transmission and controlled a variety of polarized cell behaviors [120–124]. Similar to the monitored charge that we have used in this chapter, a polarizing signal initiates polar distribution of signaling molecules and leads to polarity establishment and maintenance through the cytoskeleton and vesicular trafficking [121]. For example, during planar cell polarity (PCP) signaling, core PCP proteins are sorted asymmetrically along the polarization axis, where PCP refers to coordinated polarization of cells within the plane of a cell sheet. This sorting is thought to direct coordinated downstream morphogenetic changes across the entire tissue [123–126]. We also note that there have been other modes to achieve signal transmission, such as using the injection of finite-duration vibrational signals encoding information into a biomolecular wire of the polypeptide glycine1000 [127].

For this open field, there are still much more to be thought and to be done. Future directions might include, but not limited to, the following forefronts.

(1). The concerted orientations of the dipole molecule chains inside the nanochannels are maintained by the dipole–dipole interactions. It is expected that the "in phase" strength between those dipole orientations becomes weak as the number of dipole molecules increases. This is very important in the practice of the long-range transmission of the dipole signals. It has been shown that the correlation of the motion of the water molecules in a one-dimensional water chain confined

in the SWNT decays as the number of water molecules in this water chain increases [128]. How to achieve long correlation in the dipole orientation in practice is a huge challenge.

(2). Is there an energy transfer, and how does the energy transfer process work during such a dipole signal transmission, conduction, and multiplication? These questions are still unclear.

(3). Water molecules are very small. The devices and sensors based on water can be very small. However, the very small size of the water molecules can at the same time make the experimental realization and applications very difficult. The exploration of other larger polar molecules, such as urea, ethanol, and glycerol, to be used as media in the nanotubes is highly needed and desired.

(4). What other methods can ignite the initial dipole orientation of the monitored-water or some other molecules? Examples might be external electric fields and/or other polar molecules connected to this monitored-water. Finally, we should note that most of the progresses discussed in this short feature chapter are based on MD simulations so far. Experimental validations are therefore much needed.

1.2 Conclusion Remarks

Inspired by the biological channels called aquporins, the behavior of water inside the nanochannels has been extensively investigated. Particularly, the water channel with single-filed water is gated by external mechanical and electric signals; the water flow inside the nanochannel with single-filed water can be driven with biased direction by the static asymmetric electric field based on the ratchet effect; the water molecules inside the nanochannel with single-filed structure can even be used for signal transmission, conversion, and multiplication at the molecular level. When the radius of the nanochannel is larger, the channel can even serve as the lab-in-tube to controllably manipulate biomolecules for various applications, including chemical reaction.

Finally, we noted that most of the studies for the water inside nanochannels are experimental and numerical. Analytical study may better exploit the physics underlying, and we think this is an important direction.

References

1. Whitesides, G.M.: The origins and the future of microfluidics. Nature **442**(7101), 368–373 (2006)
2. Whitby, M., Quirke, N.: Fluid flow in carbon nanotubes and nanopipes. Nat. Nanotech. **2**(2), 87–94 (2007)
3. Squires, T.M., Quake, S.R.: Microfluidics: fluid physics at the nanoliter scale. Rev. Mod. Phys. **77**, 977 (2005)

4. Regan, B.C., Aloni, S., Ritchie, R.O., Dahmen, U., Zettl, A.: Carbon nanotubes as nanoscale mass conveyors. Nature **428**(6986), 924–927 (2004)
5. Service, R.F.: Desalination freshens up. Science **313**(5790), 1088–1090 (2006)
6. Holt, J.K., Park, H.G., Wang, Y.M., Stadermann, M., Artyukhin, A.B., Grigoropoulos, C.P., Noy, A., Bakajin, O.: Fast mass transport through sub-2-nanometer carbon nanotubes. Science **312**(5776), 1034–1037 (2006)
7. Bourlon, B., Wong, J., Miko, C., Forro, L., Bockrath, M.: A nanoscale probe for fluidic and ionic transport. Nat. Nanotech. **2**(2), 104–107 (2007)
8. Besteman, K., Lee, J.O., Wiertz, F.G.M., Heering, H.A., Dekker, C.: Enzyme-coated carbon nanotubes as single-molecule biosensors. Nano Lett. **3**, 727–730 (2003)
9. Ghosh, S., Sood, A.K., Kumar, N.: Carbon nanotube flow sensors. Science **299**(5609), 1042–1044 (2003)
10. Cambr, E.S., Schoeters, B., Luyckx, S., Goovaerts, E., Wenseleers, W.: Experimental observation of single-filed water filling of thin single-wall carbon nanotubes down to chiral index (5,3). Phys. Rev. Lett. **104**(20), 207401 (2010)
11. Falk, K., Sedlmeier, F., Joly, L., Netz, R.R., Bocquet, L.: Molecular origin of fast water transport in carbon nanotube membranes: superlubricity versus curvature dependent friction. Nano Lett. **10**(10), 4067–4073 (2010)
12. Liu, B., Li, X., Li, B., Xu, B., Zhao, Y.: Carbon nanotube based artificial water channel protein: membrane perturbation and water transportation. Nano Lett. **9**(4), 1386–1394 (2009)
13. Yuan, Q., Zhao, Y.-P.: Hydroelectric voltage generation based on water-filled single-walled carbon nanotubes. J. Am. Chem. Soc. **131**(18), 6374–6376 (2009)
14. Zhao, Y.C., Song, L., Deng, K., Liu, Z., Zhang, Z.X., Yang, Y.L., Wang, C., Yang, H.F., Jin, A.Z., Luo, Q., Gu, C.Z., Xie, S.S., Sun, L.F.: Individual water-filled single-walled carbon nanotubes as hydroelectric power converters. Adv. Mater. **20**(9), 1772 (2008)
15. Joseph, S., Aluru, N.R.: Why are carbon nanotubes fast transporters of water? Nano Lett. **8**(2), 452–458 (2008)
16. Wang, B., Král, P.: Coulombic dragging of molecules on surfaces induced by separately flowing liquids. J. Am. Chem. Soc. **128**(50), 15984–15985 (2006)
17. Majumder, M., Chopra, N., Andrews, R., Hinds, B.J.: Nanoscale hydrodynamics: enhanced flow in carbon nanotubes. Nature **438**(7064), 44–44 (2005)
18. Fang, H., et al.: Dynamics of single-file water chains inside nanoscale channels: physics, biological significance and applications. J. Phys. D Appl. Phys. **41**(10), 103002 (2008)
19. Wan, R., Fang, H.: Water transportation across narrow channel of nanometer dimension. Solid State Commun. **150**(21–22), 968–975 (2010)
20. Craighead, H.: Future lab-on-a-chip technologies for interrogating individual molecules. Nature **442**(7101), 387–393 (2006)
21. Hummer, G., Rasaiah, J.C., Noworyta, J.P.: Water conduction through the hydrophobic channel of a carbon nanotube. Nature **414**, 188–190 (2001)
22. Li, J.Y., Gong, X.J., Lu, H.J., Li, D., Fang, H.P., Zhou, R.H.: Electrostatic gating of a nanometer water channel. Proc. Natl. Acad. Sci. U. S. A. **104**, 3687–3692 (2007)
23. Zhu, F., Schulten, K.: Water and proton conduction through carbon nanotubes as models for biological channels. Biophys. J. **85**(1), 236–244 (2003)
24. Beckstein, O., Sansom, M.S.P.: Liquid–vapor oscillations of water in hydrophobic nanopores. Proc. Natl. Acad. Sci. U. S. A. **100**(12), 7063–7068 (2003)
25. Reiter, G., Burnham, C., Homouz, D., Platzman, P.M., Mayers, J., Abdul-Redah, T., Moravsky, A.P., Li, J.C., Loong, C.K., Kolesnikov, A.I.: Anomalous behavior of proton zero point motion in water confined in carbon nanotubes. Phys. Rev. Lett. **97**(24), 247801 (2006)
26. Sun, L., Crooks, R.M.: Single carbon nanotube membranes: a well-defined model for studying mass transport through nanoporous materials. J. Am. Chem. Soc. **122**(49), 12340–12345 (2000)
27. Tenne, R.: Inorganic nanotubes and fullerene-like nanoparticles. Nat. Nanotech. **1**(2), 103–111 (2006)

28. Joseph, S., Mashl, R.J., Jakobsson, E., Aluru, N.R.: Electrolytic transport in modified carbon nanotubes. Nano Lett. **3**(10), 1399–1403 (2003)
29. Denker, B.M., Smith, B.L., Kuhajda, F.P., Agre, P.: Identification, purification, and partial characterization of a novel Mr 28,000 integral membrane protein from erythrocytes and renal tubules. J. Biol. Chem. **263**(30), 15634–15642 (1988)
30. Zeidel, M.L., Ambudkar, S.V., Smith, B.L., Agre, P.: Reconstitution of functional water channels in liposomes containing purified red cell CHIP28 protein. Biochemistry **31**(33), 7436–7440 (1992)
31. Jensen, M.Ø., Tajkhorshid, E., Schulten, K.: Electrostatic tuning of permeation and selectivity in aquaporin water channels. Biophys. J. **85**(5), 2884–2899 (2003)
32. de Groot, B.L., Grubmuller, H.: Water permeation across biological membranes: mechanism and dynamics of aquaporin-1 and GlpF. Science **294**(5550), 2353–2357 (2001)
33. Chakrabarti, N., Tajkhorshid, E., Roux, B., Pomès, R.: Molecular basis of proton blockage in aquaporins. Structure **12**(1), 65–74 (2004)
34. Tajkhorshid, E., Nollert, P., Jensen, M.O., Miercke, L.J.W., O'Connell, J., Stroud, R.M., Schulten, K.: Control of the selectivity of the aquaporin water channel family by global orientational tuning. Science **296**(5567), 525–530 (2002)
35. Ilan, B., Tajkhorshid, E., Schulten, K., Voth, G.A.: The mechanism of proton exclusion in aquaporin channels. Proteins Struct. Funct. Bioinf. **55**(2), 223–228 (2004)
36. Burykin, A., Warshel, A.: What really prevents proton transport through aquaporin? Charge self-energy versus proton wire proposals. Biophys. J. **85**(6), 3696–3706 (2003)
37. Patargias, G., Bond, P.J., Deol, S.S., Sansom, M.S.P.: Molecular dynamics simulations of GlpF in a Micelle vs in a Bilayer: conformational dynamics of a membrane protein as a function of environment. J. Phys. Chem. B **109**(1), 575–582 (2004)
38. Vidossich, P., Cascella, M., Carloni, P.: Dynamics and energetics of water permeation through the aquaporin channel. Proteins Struct. Funct. Bioinf. **55**(4), 924–931 (2004)
39. Sui, H., Han, B.-G., Lee, J.K., Walian, P., Jap, B.K.: Structural basis of water-specific transport through the AQP1 water channel. Nature **414**(6866), 872–878 (2001)
40. Wan, R.Z., Li, J.Y., Lu, H.J., Fang, H.P.: Controllable water channel gating of nanometer dimensions. J. Am. Chem. Soc. **127**(19), 7166–7170 (2005)
41. Branden, C., Tooze, J.: Introduction to protein structure. Garland Publishing, New York and London (1991)
42. Xiu, P., Zhou, B., Qi, W.P., Lu, H.J., Tu, Y.S., Fang, H.P.: Manipulating biomolecules with aqueous liquids confined within single-walled nanotubes. J. Am. Chem. Soc. **131**(8), 2840–2845 (2009)
43. Gong, X.J., Li, J.Y., Lu, H.J., Wan, R.Z., Li, J.C., Hu, J., Fang, H.P.: A charge-driven molecular water pump. Nat. Nanotech. **2**, 709–712 (2007)
44. Pan, X.L., Fan, Z.L., Chen, W., Ding, Y.J., Luo, H.Y., Bao, X.H.: Enhanced ethanol production inside carbon-nanotube reactors containing catalytic particles. Nat. Mater. **6**(7), 507–511 (2007)
45. Yang, H.Q., Zhang, L., Zhong, L., Yang, Q.H., Li, C.: Enhanced cooperative activation effect in the hydrolytic kinetic resolution of Epoxides on [Co(salen)] catalysts confined in nanocages. Angew. Chem. Int. Ed. **46**(36), 6861–6865 (2007)
46. Won, C.Y., Aluru, N.R.: Water permeation through a subnanometer boron nitride nanotube. J. Am. Chem. Soc. **129**(10), 2748 (2007)
47. Eggers, D.K., Valentine, J.S.: Molecular confinement influences protein structure and enhances thermal protein stability. Protein Sci. **10**(2), 250–261 (2001)
48. Shin, K., Obukhov, S., Chen, J.T., Huh, J., Hwang, Y., Mok, S., Dobriyal, P., Thiyagarajan, P., Russell, T.P.: Enhanced mobility of confined polymers. Nat. Mater. **6**(12), 961–965 (2007)
49. Lucent, D., Vishal, V., Pande, V.S.: Protein folding under confinement: a role for solvent. Proc. Natl. Acad. Sci. U. S. A. **104**(25), 10430–10434 (2007)
50. Zhang, S.Q., Cheung, M.S.: Manipulating biopolymer dynamics by anisotropic nanoconfinement. Nano Lett. **7**(11), 3438–3442 (2007)

51. Sorin, E.J., Pande, V.S.: Nanotube confinement denatures protein helices. J. Am. Chem. Soc. **128**(19), 6316–6317 (2006)
52. Koga, K., Gao, G.T., Tanaka, H., Zeng, X.C.: Formation of ordered ice nanotubes inside carbon nanotubes. Nature **412**(6849), 802–805 (2001)
53. Noon, W.H., Ausman, K.D., Smalley, R.E., Ma, J.P.: Helical ice-sheets inside carbon nanotubes in the physiological condition. Chem. Phys. Lett. **355**(5–6), 445–448 (2002)
54. Mashl, R.J., Joseph, S., Aluru, N.R., Jakobsson, E.: Anomalously immobilized water: a new water phase induced by confinement in nanotubes. Nano Lett. **3**(5), 589–592 (2003)
55. Striolo, A.: The mechanism of water diffusion in narrow carbon nanotubes. Nano Lett. **6**(4), 633–639 (2006)
56. Raghavender, U.S., Kantharaju, Aravinda, S., Shamala, N., Balaram, P.: Hydrophobic peptide channels and encapsulated water wires. J. Am. Chem. Soc. **132**(3), 1075–1086 (2010)
57. Reddy, G., Straub, J.E., Thirumalai, D.: Dry amyloid fibril assembly in a yeast prion peptide is mediated by long-lived structures containing water wires. Proc. Natl. Acad. Sci. U. S. A. **107**(50), 21459–21464 (2010)
58. Xiu, P., Yang, Z.X., Zhou, B., Das, P., Fang, H.P., Zhou, R.H.: Urea-induced drying of hydrophobic nanotubes: comparison of different urea models. J. Phys. Chem. B **115**(12), 2988–2994 (2011)
59. Tu, Y., Xiu, P., Wan, R., Hu, J., Zhou, R., Fang, H.: Water-mediated signal multiplication with Y-shaped carbon nanotubes. Proc. Natl. Acad. Sci. U. S. A. **106**(43), 18120–18124 (2009)
60. Dokter, A.M., Woutersen, S., Bakker, H.J.: Anomalous slowing down of the vibrational relaxation of liquid water upon nanoscale confinement. Phys. Rev. Lett. **94**(17), 178301 (2005)
61. Ju, S.P., Yang, S.H., Liao, M.L.: Study of molecular behavior in a water nanocluster: size and temperature effect. J. Phys. Chem. B **110**(18), 9286–9290 (2006)
62. Vaitheeswaran, S., Thirumalai, D.: Hydrophobic and ionic interactions in nanosized water droplets. J. Am. Chem. Soc. **128**(41), 13490–13496 (2006)
63. Sykes, M.T., Levitt, M.: Simulations of RNA base pairs in a nanodroplet reveal solvation-dependent stability. Proc. Natl. Acad. Sci. U. S. A. **104**(30), 12336–12340 (2007)
64. Yeh, I.C., Hummer, G.: Nucleic acid transport through carbon nanotube membranes. Proc. Natl. Acad. Sci. U. S. A. **101**(33), 12177–12182 (2004)
65. Zimmerli, U., Koumoutsakos, P.: Simulations of electrophoretic RNA transport through transmembrane carbon nanotubes. Biophys. J. **94**(7), 2546–2557 (2008)
66. Insepov, Z., Wolf, D., Hassanein, A.: Nanopumping using carbon nanotubes. Nano Lett. **6**(9), 1893–1895 (2006)
67. Longhurst, M.J., Quirke, N.: Temperature-driven pumping of fluid through single-walled carbon nanotubes. Nano Lett. **7**(11), 3324–3328 (2007)
68. Wang, Z.K., Ci, L.J., Chen, L., Nayak, S., Ajayan, P.M., Koratkar, N.: Polarity-dependent electrochemically controlled transport of water through carbon nanotube membranes. Nano Lett. **7**(3), 697–702 (2007)
69. Savariar, E.N., Krishnamoorthy, K., Thayumanavan, S.: Molecular discrimination inside polymer nanotubules. Nat. Nanotech. **3**(2), 112–117 (2008)
70. Kral, P., Tomanek, D.: Laser-driven atomic pump. Phys. Rev. Lett. **82**(26), 5373–5376 (1999)
71. Balbach, J.J., Ishii, Y., Antzutkin, O.N., Leapman, R.D., Rizzo, N.W., Dyda, F., Reed, J., Tycko, R.: Amyloid fibril formation by A beta(16–22), a seven-residue fragment of the Alzheimer's beta-amyloid peptide, and structural characterization by solid state NMR. Biochemistry **39**(45), 13748–13759 (2000)
72. Bonomi, M., Gervasio, F.L., Tiana, G., Provasi, D., Broglia, R.A., Parrinello, M.: Insight into the folding inhibition of the HIV-1 protease by a small peptide. Biophys. J. **93**(8), 2813–2821 (2007)
73. Bandaru, P.R., Daraio, C., Jin, S., Rao, A.M.: Novel electrical switching behaviour and logic in carbon nanotube Y-junctions. Nat. Mater. **4**(9), 663–666 (2005)
74. Bachtold, A., Hadley, P., Nakanishi, T., Dekker, C.: Logic circuits with carbon nanotube transistors. Science **294**(5545), 1317–1320 (2001)

75. Fan, R., Yue, M., Karnik, R., Majumdar, A., Yang, P.D.: Polarity switching and transient responses in single nanotube nanofluidic transistors. Phys. Rev. Lett. **95**(8), 086607 (2005)
76. Chen, F., Hihath, J., Huang, Z., Li, X., Tao, N.J.: Measurement of single-molecule conductance. Annu. Rev. Phys. Chem. **58**(1), 535–564 (2007)
77. Heath, J.R.: Molecular electronics. Annu. Rev. Mater. Res. **39**(1), 1–23 (2009)
78. Drummond, T., Hill, M., Barton, J.: Electrochemical DNA sensors. Nat. Biotechnol. **21**(10), 1192–1199 (2003)
79. Yuan, G.D., Zhang, W.J., Jie, J.S., Fan, X., Zapien, J.A., Leung, Y.H., Luo, L.B., Wang, P.F., Lee, C.S., Lee, S.T.: p-Type ZnO nanowire arrays. Nano Lett. **8**(8), 2591–2597 (2008)
80. Kong, J., Franklin, N., Zhou, C., Chapline, M., Peng, S., Cho, K., Dai, H.: Nanotube molecular wires as chemical sensors. Science **287**(5453), 622–625 (1999)
81. Cui, Y., Wei, Q., Park, H., Lieber, C.: Nanowire nanosensors for highly sensitive and selective detection of biological and chemical species. Science **293**(5533), 1289 (2001)
82. Li, D., Song, S., Fan, C.: Target-responsive structural switching for nucleic acid-based sensors. Acc. Chem. Res. **43**(5), 631–641 (2010)
83. Bennett, M., Zukin, R.: Electrical coupling and neuronal synchronization in the mammalian brain. Neuron **41**(4), 495–511 (2004)
84. Connors, B., Long, M.: Electrical synapses in the mammalian brain. Annu. Rev. Neurosci. **27**, 393–418 (2004)
85. Bartos, M., Vida, I., Jonas, P.: Synaptic mechanisms of synchronized gamma oscillations in inhibitory interneuron networks. Nat. Rev. Neurosci. **8**(1), 45–56 (2007)
86. Söhl, G., Maxeiner, S., Willecke, K.: Expression and functions of neuronal gap junctions. Nat. Rev. Neurosci. **6**, 191 (2005)
87. Hormuzdi, S., Pais, I., LeBeau, F., Towers, S., Rozov, A., Buhl, E., Whittington, M., Monyer, H.: Impaired electrical signaling disrupts gamma frequency oscillations in Connexin 36-Deficient Mice. Neuron **31**, 487–495 (2001)
88. Amitai, Y., Gibson, J., Beierlein, M., Patrick, S., Ho, A., Connors, B., Golomb, D.: The spatial dimensions of electrically coupled networks of interneurons in the neocortex. J. Neurosci. **22**(10), 4142 (2002)
89. Zoidl, G., Dermietzel, R.: On the search for the electrical synapse: a glimpse at the future. Cell Tissue Res. **310**(2), 137–142 (2002)
90. Pfeuty, B., Mato, G., Golomb, D., Hansel, D.: Electrical synapses and synchrony: the role of intrinsic currents. J. Neurosci. **23**(15), 6280 (2003)
91. Smock, R.G., Gierasch, L.M.: Sending signals dynamically. Science **324**(5924), 198–203 (2009)
92. Tsai, C.-J., del Sol, A., Nussinov, R.: Allostery: absence of a change in shape does not imply that allostery is not at play. J. Mol. Biol. **378**(1), 1–11 (2008)
93. Tsai, C., Sol, A., Nussinov, R.: Protein allostery, signal transmission and dynamics: a classification scheme of allosteric mechanisms. Mol. Biosyst. **5**(3), 207–216 (2009)
94. Sethna, J.: Statistical mechanics: entropy, order parameters, and complexity. Oxford University Press, USA (2006)
95. Dudko, O.: Statistical mechanics: entropy, order parameters, and complexity. J. Stat. Phys. **126**(2), 429–430 (2007)
96. de Jonge, J.J., Ratner, M.A., de Leeuw, S.W., Simonis, R.O.: Molecular dipole chains III: energy transfer. J. Phys. Chem. B **108**(8), 2666–2675 (2004)
97. de Jonge, J.J., Ratner, M.A., de Leeuw, S.W., Simonis, R.O.: Controlling the energy transfer in dipole chains. J. Phys. Chem. B **110**(1), 442–446 (2005)
98. de Jonge, J.J., Ratner, M.A., de Leeuw, S.W.: Local field controlled switching in a one-dimensional dipolar array. J. Phys. Chem. C **111**(9), 3770–3777 (2007)
99. Ball, P.: Water as an active constituent in cell biology. Chem. Rev. **108**(1), 74–108 (2008)
100. Zhou, R.H., Huang, X.H., Margulis, C.J., Berne, B.J.: Hydrophobic collapse in multidomain protein folding. Science **305**(5690), 1605–1609 (2004)
101. Brewer, M.L., Schmitt, U.W., Voth, G.A.: The formation and dynamics of proton wires in channel environments. Biophys. J. **80**(4), 1691–1702 (2001)

102. Pomes, R., Roux, B.: Molecular mechanism of H+ conduction in the single-file water chain of the gramicidin channel. Biophys. J. **82**(5), 2304–2316 (2002)
103. Beckstein, O., Biggin, P.C., Sansom, M.S.P.: A hydrophobic gating mechanism for nanopores. J. Phys. Chem. B **105**(51), 12902–12905 (2001)
104. Köfinger, J., Hummer, G., Dellago, C.: Macroscopically ordered water in nanopores. Proc. Natl. Acad. Sci. U. S. A. **105**(36), 13218–13222 (2008)
105. Berendsen, H.J.C., Postma, J.P.M., van Gunsteren, W.F., DiNola, A., Haak, J.R.: Molecular dynamics with coupling to an external bath. J. Chem. Phys. **81**(8), 3684–3690 (1984)
106. Berendsen, H.J.C., van der Spoel, D., van Drunen, R.: GROMACS: a message-passing parallel molecular dynamics implementation. Comput. Phys. Commun. **91**(1–3), 43–56 (1995)
107. Hua, L., Zhou, R., Thirumalai, D., Berne, B.: Urea denaturation by stronger dispersion interactions with proteins than water implies a 2-stage unfolding. Proc. Natl. Acad. Sci. U. S. A. **105**(44), 16928 (2008)
108. Lindahl, E., Hess, B., van der Spoel, D.: GROMACS 3.0: a package for molecular simulation and trajectory analysis. J. Mol. Model. **7**(8), 306–317 (2001)
109. Zhou, R.: Exploring the protein folding free energy landscape: coupling replica exchange method with P3ME/RESPA algorithm. J. Mol. Graph. Model **22**(5), 451–463 (2004)
110. Hua, L., Huang, X., Zhou, R., Berne, B.J.: Dynamics of water confined in the interdomain region of a multidomain protein. J. Phys. Chem. B **110**(8), 3704–3711 (2006)
111. Liu, P., Huang, X., Zhou, R., Berne, B.J.: Hydrophobic aided replica exchange: an efficient algorithm for protein folding in explicit solvent. J. Phys. Chem. B **110**(38), 19018–19022 (2006)
112. Darden, T., York, D., Pedersen, L.: Particle mesh Ewald: an N [center-dot] log(N) method for Ewald sums in large systems. J. Chem. Phys. **98**(12), 10089–10092 (1993)
113. Papadopoulos, C., Rakitin, A., Li, J., Vedeneev, A.S., Xu, J.M.: Electronic transport in Y-junction carbon nanotubes. Phys. Rev. Lett. **85**(16), 3476 (2000)
114. Satishkumar, B.C., Thomas, P.J., Govindaraj, A., Rao, C.N.R.: Y-junction carbon nanotubes. Appl. Phys. Lett. **77**(16), 2530–2532 (2000)
115. Li, W.Z., Wen, J.G., Ren, Z.F.: Straight carbon nanotube Y junctions. Appl. Phys. Lett. **79**(12), 1879–1881 (2001)
116. Deepak, F.L., Govindaraj, A., Rao, C.N.R.: Synthetic strategies for Y-junction carbon nanotubes. Chem. Phys. Lett. **345**(1–2), 5–10 (2001)
117. Terrones, M., Banhart, F., Grobert, N., Charlier, J.C., Terrones, H., Ajayan, P.M.: Molecular junctions by joining single-walled carbon nanotubes. Phys. Rev. Lett. **89**(7), 075505 (2002)
118. Gothard, N., Daraio, C., Gaillard, J., Zidan, R., Jin, S., Rao, A.M.: Controlled growth of Y-junction nanotubes using Ti-Doped vapor catalyst. Nano Lett. **4**(2), 213–217 (2004)
119. Liu, P., Huang, X., Zhou, R., Berne, B.: Observation of a dewetting transition in the collapse of the melittin tetramer. Nature **437**(7055), 159–162 (2005)
120. Søgaard-Andersen, L.: Cell polarity, intercellular signalling and morphogenetic cell movements in Myxococcus xanthus. Curr. Opin. Microbiol. **7**(6), 587–593 (2004)
121. Yang, Z.: Cell polarity signaling in Arabidopsis. Annu. Rev. Cell Dev. Bi. **24**, 551–575 (2008)
122. Fuller-Espie, S., Hoffman Towler, P., Wiest, D., Tietjen, I., Spain, L.: Transmembrane polar residues of TCR beta chain are required for signal transduction. Int. Immunol. **10**(7), 923 (1998)
123. Jones, C., Roper, V.C., Foucher, I., Qian, D., Banizs, B., Petit, C., Yoder, B.K., Chen, P.: Ciliary proteins link basal body polarization to planar cell polarity regulation. Nat. Genet. **40**(1), 69–77 (2008)
124. Ganner, A., Lienkamp, S., Schäfer, T., Romaker, D., Wegierski, T., Park, T., Spreitzer, S., Simons, M., Gloy, J., Kim, E.: Regulation of ciliary polarity by the APC/C. Proc. Natl. Acad. Sci. U. S. A. **106**(42), 17799 (2009)
125. Axelrod, J.: Unipolar membrane association of Dishevelled mediates Frizzled planar cell polarity signaling. Gene. Dev. **15**(10), 1182 (2001)

126. Mitchell, B., Jacobs, R., Li, J., Chien, S., Kintner, C.: A positive feedback mechanism governs the polarity and motion of motile cilia. Nature **447**(7140), 97–101 (2007)
127. Miao, L., Seminario, J.: Molecular dynamics simulations of signal transmission through a glycine peptide chain. J. Chem. Phys. **127**, 134708 (2007)
128. Li, J.-Y., Yang, Z.-X., Fang, H.-P., Zhou, R.-H., Tang, X.-W.: Effect of the carbon-nanotube length on water permeability. Chin. Phys. Lett. **24**(9), 2710–2713 (2007)
129. Lu, H., Li, J., Gong, X., Wan, R., Zeng, L., Fang, H.: Water permeation and wavelike density distributions inside narrow nanochannels. Phys. Rev. B **77**(17), 174115 (2008)
130. Lu, H.-J., Gong, X.-J., Wang, C.-L., Fang, H.-P., Wan, R.-Z.: Effect of vibration on water transport through carbon nanotubes. Chin. Phys. Lett. **25**(3), 1145–1148 (2008)
131. Wu, L., Wu, F., Kou, J., Lu, H., Liu, Y.: Effect of the position of constriction on water permeation across a single-walled carbon nanotube. Phy. Rev. E **83**(6), 061913 (2011)
132. Tu, Y., Zhou, R., Fang, H.: Signal transmission, conversion and multiplication by polar molecules confined in nanochannels. Nanoscale **2**(8), 1976–1983 (2010)